Article:
Pei, Y, Paton, DA, Knipe, RJ et al. (3 more authors) (2018) Unraveling the influence of throw and stratigraphy in controlling subseismic fault architecture of fold-thrust belts: An example from the Qaidam Basin, northeast Tibetan Plateau. AAPG Bulletin, 102 (6). pp. 1091-1117. ISSN 0149-1423

https://doi.org/10.1306/08101716503

Unravelling the influence of throw and stratigraphy in controlling sub-seismic fault architecture of fold-thrust belts: an example from the Qaidam Basin, NE Tibetan Plateau

Yangwen Pei[a, b, e *], Douglas A. Paton[b, *], Rob J. Knipe[b],

W. Henry Lickorish[c], Anren Li[d], Kongyou Wu[a]

[a] School of Geosciences, China University of Petroleum, Qingdao, 266580, China

[b] School of Earth & Environment, University of Leeds, Leeds, West Yorkshire, LS2 9JT, UK

[c] 22 140 Point Drive NW, Calgary T3D 4W3, Canada

[d] Central Area Exploration Division, Saudi Aramco, Dhahran, 31311, Kingdom of Saudi Arabia

[e] Key Laboratory of Tectonics and Petroleum Resources, Ministry of Education, Wuhan 430074, China

[*] Corresponding authors: Y. Pei: peiyangwen@upc.edu.cn / D.A. Paton: d.a.paton@leeds.ac.uk

Acknowledgements

We would like to thank our colleagues Dr. Geoff Lloyd, Dr. Jonathan Imber, and Dr. Liu-juan Xie for the extensive discussions and suggestions that have contributed to this research. Discussion and support from Dr. Pengju Li, Rock Deformation Research Ltd. and the Qinghai Oilfield of PetroChina is also appreciated. The VSA (Virtual Seismic Atlas) is also thanked for allowing use of the seismic data of the Niger Delta. Thanks are also given to AAPG Editor Dr. Barry J. Katz, Senior Associate Editor Dr. Caroline Burberry and three reviewers (Dr. Kara L English, Dr. Avraam Zelilidis, and Dr. Andrés R Mora) for their constructive comments that helped improve this manuscript significantly. This work has been collaboratively supported by the National Natural Science Foundation of China (NO.41502192, NO.41272142, NO.41602143), the Shandong Provincial Natural Science Foundation China (NO.2014BSE28008), and the Open Funding of the Key Laboratory of Tectonics and Petroleum Resources (NO.TPR-2016-02).

Abstract

Understanding the detailed fault architecture of reverse faulting is critical for understanding the processes involved in fold-thrust belts as well as predicting the degree of fault compartmentalisation, the relationship between folds and faults, the distribution of strain and sub-seismic faulting deformation. The Lenghu5 fold-thrust belt, provides an exceptionally well-exposed outcrop example of a reverse fault-related fold. Detailed stratigraphic logging coupled with high-resolution cross-sections provides a unique insight into the 3D geometry of a thrust fault at both basin and outcrop scale. In this study we observe that 85 - 90% of the estimated throw is accommodated on the main fault zone, which has sufficient throw to be imaged on a seismic profile, while 15-20% of the throw is accommodated on smaller scale folds and faults that are beyond seismic resolution. The plan view mapping of the structure reveals that there is significant variation in how strain is accommodated along the structure, which is associated with the throw variations in the main fault. In addition, by coupling the structural observations within a stratigraphic context, we can demonstrate that although the main fault controls the overall strain in the system, the local stratigraphy plays a critical role in how the strain is accommodated and whether it is partitioned into single faults, multiple-fault splays or folding. By demonstrating the remarkable geometric similarity between the outcrop observations with a comparable structure in the sub-surface (Niger Delta), the study provides an insight into the potential sub-seisimic fault zone geometry present in poorly imaged fold-thrust systems.

Keywords

fault architecture, sub-seismic structures, lateral structural variation, scale dependence

1. Introduction

Understanding fault architecture at an outcrop scale is fundamental as it controls the fault zone compartmentalization which impacts fluid flow properties across fault zones (e.g., Childs et al., 2007; Torabi and Fossen, 2009; Fokker et al., 2012; Alves and Elliott, 2014;

Pei et al., 2015; Place et al., 2016). Many studies focusing on fault processes (Caine et al., 1996; Childs et al., 1996b; Rotevatn et al., 2007; Childs et al., 2009), fault geometry (Peacock and Sanderson, 1991, 1992, 1994) and fault populations (Cowie and Scholz, 1992; Cowie et al., 1993; Cowie et al., 1996; Kolyukhin et al., 2010; Fossen and Rotevatn, 2016) have provided insights in detailed fault architecture and significantly improved the accuracy of risk assessment in hydrocarbon exploration and development. Although the relationship between faults and folds developed within compressional systems is well established (e.g., Bally et al., 1966; Price, 1981; Coward, 1983b, a; Barclay and Smith, 1992; Yin et al., 2008b; Roche et al., 2012; Brandes and Tanner, 2014; Pei et al., 2014), the detailed fault architecture of thrust faults remain poorly constrained, particularly at the meso-scale and assessing seismic data. Not only are sub-seismic faults poorly imaged but even seismically resolvable structures are poorly imaged because of the steep dipping nature of reflections (Iacopini and Butler, 2011; Iacopini et al., 2012; Alcalde et al., 2017), which makes it difficult to predict the fault zone geometry in detail, particularly the prediction of sub-seismic faulting and compartmentalisation in thrust systems.

In order to investigate thrust fault architecture, we have studied the detailed (10 m / 32.8 ft - 10 km / 6.21 mi scale) fault architecture of an exceptionally well exposed fold-thrust belt in the Lenghu5 fold-thrust belt of the Qaidam Basin, N.E. Tibetan Plateau, that is controlled by compressional deformation (e.g., Allen and Vincent, 1997; Yin et al., 2008a; Yin et al., 2008b; Liu et al., 2009). Here we provide a high-resolution fault architecture analysis of a thrust fault zone in the Qaidam basin for the first time using the exceptionally exposed Lenghu5 system. Stratigraphic logging and cross section construction are used to quantitatively understand the structural geometry and the lateral variation of structural elements along this feature. 3D geospatial models are built to evaluate the controlling parameters of the structural variation of the Lenghu5 fold-thrust belt.

Trishear propagation models have been previously used at Lenghu5 to examine the structural geometry and evolution on seismic profiles (e.g., Pei et al., 2014; Pei et al., 2017b), but the detailed fault architecture, that is poorly imaged on seismic profiles, has not been properly interpreted in detail and there is significant uncertainty in respect to the strain distribution within the poorly imaged zone. By comparing our results with an equivalent fold-thrust belt system in the deep water Niger Delta, we propose that our study is applicable to helping sub-surface fault prediction in poorly imaged fold-thrust systems.

2. Geological Setting

The Qaidam Basin is triangular in plan view, with a ~ 550 km / 341.8 mi NE margin, a ~ 300 km / 186.4 mi NW margin and a ~ 700 km / 435.0 mi SW margin (**Fig. 1a**). The basin, with an average elevation of ~ 2800 m / 1.74 mi above mean sea-level, is constrained by the QilianShan-NanShan Thrust Belt to the northeast (e.g. Burchfiel et al., 1989; Tapponnier et al., 1990; Yin et al., 2008a), the Altyn Tagh Strike-slip Fault to the northwest (e.g. Meyer et al., 1998; Cowgill et al., 2000; Yin et al., 2007) and the QimenTagh-EasternKunlun Thrust Belt to the southwest (e.g. Jolivet et al., 2003; Yin et al., 2007; Wu et al., 2011). The basin, as illustrated in the NE-SW orientated cross-section in **Fig. 1b** (modified from Yin et al., 2008b), contains up to 16 km / 9.94 mi thickness of Cenozoic sediments (E_{1+2}-Q_1) and locally-distributed thin Mesozoic sediments (Jr). The ~ 190 km / 118.1 mi cross-section demonstrates that the first order syncline in the Qaidam Basin (**Fig. 1b**) comprises a series of tight anticlines and open synclines, while subordinate structures (at scales of 100 m / 328.1 ft -1 km / 0.62 mi) are smaller scale folds/faults. The syn-kinematic sedimentation is evident in the basin and reveals a complex geological history for the Qaidam Basin that comprises both extension in the Mesozic and compression in the Cenozoic. The thickening of Cenozoic sediments within the centre of the basin suggests the Qaidam Basin is controlled by NE-SW compression resulting from the uplift of the Tibetan Plateau (e.g., Molnar and Tapponnier, 1975; Xia et al., 2001; Pang et al., 2004; Wang and Burchfiel, 2004; Wang et al., 2006b; Zhou et al., 2006; Zhu et al., 2006). Estimates of total shortening of the central Qaidam Basin (Zhou et al., 2006; Yin et al., 2008b; Liu et al., 2009), since 65 Ma is 20 ± 2 km (12.4 ± 1.24 mi), implying a shortening rate of 0.30 ± 0.04 mm/a (0.0118 ± 0.0016 in/a). In this study we focus on the Lenghu5 fold-thrust belt (e.g., Wu et al., 2011; Pei et al., 2014), located in northern Qaidam Basin, which is a ~ 10 km / 6.21 mi wide asymmetric anticline controlled by northeast verging thrust faults (see position in **Fig. 1b**).

The geometry of the Lenghu5 anticline, which is within the hangingwall of the controlling fault, is constrained by a ~ 7 km / 4.35 mi long seismic section through the Lenghu5 fold-thrust belt (**Fig. 1c**) while the internal stratigraphy is well constrained by the Lengke1 well (data from Yang et al., 2003; Pang et al., 2004; Pei et al., 2014). The Lenghu5 surface geology shows a broad fold cut by a high-angle thrust fault through the fold axis (**Fig. 1c**). However, the seismic section suggests shallowing of the dip of the thrust fault with increasing depth into a décollement above a sequence interpreted as late Eocene sediments (E_3). The Lenghu5 anticline extends throughout the section continuing below the thrust fault. The origin of the Lenghu5 anticline is attributed to the regional NE-SW oriented compression (e.g., Chen et al., 2005; Wang et al., 2006a; Pei et al., 2014). The Lenghu5 anticline is controlled by the lower SW-directing reactivated faults (F_a and F_b) and the upper younger NE-directing thrust fault (F_c). The two main faults F_c and F_a account for the majority of the fault throw: ~ 800 m / 0.49 mi throw in the unit J_r along F_a and ~ 800 m / 0.49 mi in the unit N_1 along F_c.

This study integrated surface and shallow subsurface data of the Lenghu5 fold-thrust belt (see the blue rectangle in **Fig. 1c**), thus, we focus on the control of fault zone throw on structural variation along strike of the Lenghu5 fold-thrust belt. The distribution of fault zone throw was evaluated to understand its control on structural variation along strike of the Lenghu5 fold-thrust belt. The Lenghu5 area presents well-exposed outcrops of the central fault zone and its adjacent hanging-wall and footwall, which provides the platform for the two sets of high-resolution fieldwork used to investigate the detailed fault zone architecture.

3. Data and Methods

For the analysis of the Lenghu5 fold-thrust belt we have integrated both remote sensing data (landsat images) and field observations, which are outlined below, to derive a 3D geospatial model (Paton et al., 2007). We applied the following data collection and analysis techniques:

1) Stratigraphy logging: to constrain the detailed stratigraphy within the Lenghu5 fold-thrust belt three well exposed traverses (2150 m / 1.34 mi total stratigraphic thickness) across the structure were logged; this corresponds to HW1, HW2 and FW, representing hanging-wall section 1, hanging-wall section 2, and footwall section, respectively (**Fig. 2**).

2) Cross section construction: to investigate the spatial distribution of throw along the fault zone and the anticline geometry in the hanging-wall, ten parallel sections were created based on detailed structural measurements and ground-truthed satellite image interpretation (**Figs. 3** - **6**) (see also Watkins et al., 2017). For cross section construction, it was assumed that layer cake stratigraphy was appropriate based upon the continuous stratigraphic units mapped out on the landsat image and the stratigraphic logs. The detailed stratigraphic profiles were projected onto the section topography to assist the stratigraphy construction. The stratigraphic boundaries were extrapolated above the present topography to predict the thrust zone fault cut-off positions, which are subsequently used to estimate the throw of the fault zone. Different methods of stratigraphic extrapolation will obviously affect the subsequent throw estimation, therefore, the uncertainty of fault throw estimation was also considered (see the right side chart in **Fig. 5**). Mapping of the landsat imagery and the regional cross sections were used to analyse the fault systems at variable scales in the Lenghu5 fold-thrust belt.

3) 3D geosaptial modelling: The 3D geospatial models were constructed by integrating the field-scale observation and cross sections (**Figs. 7** - **9**). This study integrates the surface and shallow subsurface data of the Lenghu5 fold-thrust belt (see the blue rectangle in **Fig. 1c**), to focus on the control of the overall fault zone throw on structural variation along strike of the Lenghu5 fold-thrust belt. The distribution of the overall fault zone throw of the Lenghu5 thrust fault zone was analyzed by including an assessment of the fault throw. The spatial distribution of fault throw and the lateral variation of hanging-wall anticline were then quantitatively analysed to understand the 3D fault architecture of the Lenghu5 fold-thrust belt.

4) Sub-surface equivalent: A geometrically and scale equivalent example of a deep water fold-thrust belt from the Niger Delta (**Figs. 10-12**) was used to compare the field-scale observation from the Lenghu5 fold-thrust belt. Both the primary geometry and detailed dip variation in plan view maps and sections are investigated. In particular, we focus on the issue of prediction of sub-seismic fault architecture within a poorly imaged fault zone.

4. Field-scale Observation

The field observations allowed the integration of multiple geologic data (e.g., stratigraphic logs, regional cross sections with structural measurements and structural maps) to investigate the geometry of the hanging-wall anticline and the fault zone in the Lenghu5 fold-thrust belt. The field-scale observations reveal an overall geometry of two NW-SE-trending anticlines with a dominant SW-dipping thrust fault zone beneath the anticlines.

4.1. Stratigraphy

The study area exposes stratigraphy primarily of Neogene age sediments. The stratigraphy of hangingwall section 1 (**HW1**) and hangingwall section 2 (**HW2**) are similar to each other, except for the additional stratigraphic section exposed in the southern culmination (**Fig. 2, Fig. 3**). Based on the stratigraphic correlation between hanging-wall and footwall, the Lenghu5 stratigraphy has been subdivided into the following five packages: (i). $\mathbf{S_a}$

comprises fine sandstones and red/grey/mottled shales/mudstones, with a minimum thickness of 170 m / 0.11 mi in HW1; (ii). **S_b** is fine-medium sandstone interbedded with occasional thin red/grey mudstones and its thickness is ~ 350 m / 0.22 mi; (iii). **S_c** is homogeneous fine sandstone with a variable thickness (10 m / 32.8 ft - 30 m / 98.4 ft); (iv). **S_d**, ~ 400 m / 0.25 mi thick, shows a similar lithology as S_b, but with thin medium-coarse sandstone interbedded; (v). **S_e** is a coarse-very coarse sandstone, with a thickness that exceeds 250 m / 0.16 mi. The throw on the main fault zone, derived from the stratigraphic correlation between hanging-wall and footwall, is estimated to be 500 ± 20 m (0.31 ± 0.01 mi) and, therefore, is seismically resolvable and corresponds to Fc on the seismic section (**Fig. 1c**).

4.2. Regional Cross Sections

The Lenghu5 fold-thrust belt has previously been restored using a trishear algorithm in previous studies (e.g., Pei et al., 2014; Pei et al., 2017b). Based on the structural restoration, we found that, due to the reactivation of the deeper normal faults, folds were propably developed earlier than the Lenghu thrust (F_c) faulting deformation in upper section (**Fig. 1c**). That is, the folding deformation we observed in surface and shallow subsurface was related to deeper faulting deformation (F_a and F_b). In order to evaluate the contribution of folding and faulting deformation to the overall strain in the Lenghu5 fold-thrust belt, the restoration tools 'Move on Fault' and 'Unfolding' (Move, Midland Valley 2013) were employed to estimate the section shorterning due to folding and faulting, respectively (**Fig. 4**). The fault throw on the Lenghu thrust (F_c) was restored using the algorithm of 'fault parallel flow' (Egan et al., 1997), which shows section shortening of ~ 1.03 km / 3.38 ft (**Fig. 4a→b**). The section was then unfolded using the algorithm of 'flexural' (Kane et al., 1997), representing section shortening of ~ 0.51 km / 1.67 ft (**Fig. 4b→c**). Therefore, at regional scale, the overall section shortening (~ 1.54 km / 5.05 ft) was ~ 33% accounted by folding and ~ 67% accounted by faulting. However, when it comes to a more meso-scale study area (the blue rectangle in **Fig. 4a**), folding and faulting deformation accounted for section shortening of ~ 0.86 km / 2.82 ft and ~ 0.24 km / 0.79 ft. In this meso-scale scenario, faulting deformation (~ 80%) accounted for more contribution to the overall strain than folding deformation (~ 20%).

Interpretation of the landsat image reveals that the Lenghu5 structure is dominated by two anticlines, therefore, we located our two principle cross-sections (S3 and S9; **Fig. 3**) through the middle of each of the folds, perpendicular to the fold axial trace, to demonstrate the geometry and overall fault throw variation of the Lenghu5 fold-thrust belt (**Fig. 5**). The uncertainty of fault throw estimation was considered (see the right side chart in **Fig. 5**), because different methods of stratigraphic extrapolation will obviously affect the subsequent throw estimation. In the two sections S3 and S9, an anticline developed in the hanging-wall, which is a consequence of the NE verging thrust zone. To quantify the throw of the main fault zone ($\mathbf{f_1}$), the overall fault zone throw at different stratigraphic intervals are plotted to the right of the sections. These plots reveal both the vertical variation of fault throw in an individual section and lateral variation of fault zone throw between sections.

Section S3, through the northern anticline, shows a fault zone comprising the main thrust fault $\mathbf{f_1}$ and a splay fault $\mathbf{f_2}$ in the footwall (**Fig. 5a**). The hanging-wall, footwall and central fault zone, comprise strata package Sa-Se and form an assymetric anticline verging towards the NE. The hanging-wall consists of SW-dipping strata, in which the layers are progressively clockwise rotated towards the top of the fold with a corresponding decreasing dip from 45º to 10º close to the fold hinge area and fault zone. The strata are gently SW-dipping (0-10°) in the immediate hanging-wall adjacent to the main fault $\mathbf{f_1}$. In the footwall to the fault zone, the strata are gently (~ 12°) NE-dipping directly next to the splay fault $\mathbf{f_2}$, and become slightly shallower away from the fault zone. In the central fault zone between $\mathbf{f_1}$ and $\mathbf{f_2}$ the strata are observed to have a rapid change in dip from high-angle

NE-dipping (up to 70°) next to $\mathbf{f_1}$ to 10°- 15° NE-dipping next to $\mathbf{f_2}$. This dip variation within the fault zone demonstrates a higher degree of deformation of the central fault zone than the adjacent hanging-wall and footwall. The overall throw ($\mathbf{f_1}$ hanging wall to $\mathbf{f_2}$ footwall) is ~ 465 m ± 20m (~ 0.29 mi ± 0.01 mi) at the base of the unit Sa. The main fault zone, $\mathbf{f_1}$, appears to accommodate the majority of the deformation with a throw of ~ 415 m / 0.26 mi (~ 90% of the cumulative throw) while the splay fault $\mathbf{f_2}$ has a throw of ~ 50 m / 0.03 mi (~ 10% of the cumulative throw). However, the individual faults do not maintain a constant throw vertically through the section. The fault zone $\mathbf{f_1}$ decreases its throw to ~ 370 m / 0.23 mi in unit Sb, and down to ~ 210 m / 0.13 mi in unit Sc/Sd/Se (± 23 m / 75.5 ft due to the uncertainty of stratigraphic extrapolation) (see the right side-chart in **Fig. 5a**).

Section S9 through the southern anticline is in an equivalent position on the fold culmination as S3 was in the northern anticline. The fault zone in Section S9 comprises the same main thrust fault ($\mathbf{f_1}$) as observed in S3 as well as an inferred splay fault $\mathbf{f_3}$ that is accounting for the development of a smaller scale anticline (amplitude: ~ 200m / 0.12 mi; half-wavelength: > 2km / 1.2 mi) in the footwall. However, the splay fault $\mathbf{f_3}$ is blind and is not exposed at the present day topography (**Fig. 5b**). Compared with S3, the Lenghu5 fold-thrust belt in section S9 presents a more complex geometry. The hanging-wall, which presents an anticlinal geometry, has a relative flat crest adjacent to the main thrust fault $\mathbf{f_1}$. The Lenghu5 fold-thrust belt has an asymmetric geometry, with dip up to 76°SW (overturned) in the NE limb compared to dip of 10°- 34°SW in the SW limb and its geometry conforms to a fault propagation fold (e.g., Suppe and Medwedeff, 1990), where more strain is taken up by folding. The hanging-wall geometry has been successfully restored using a trishear algorithm in Pei et al. (2017b), using an apical angle of 50°, a propagation/slip ratio of 2.0, and upward-steepening fault dips of 5° - 60°. In the footwall, a small-scale tight syncline and open anticline pairs are developed, which can be attributed to the existence of the underlying blind splay fault $\mathbf{f_3}$. Projection of the horizons produce a cumulative throw of ~ 980 m / 0.61 mi across the entire fault zone ($\mathbf{f_1}$ hanging wall to $\mathbf{f_2}$ footwall). The main thrust fault $\mathbf{f_1}$ accounts for the majority of the throw: ~ 840 m / 0.52 mi in unit Sa-Sd (± 30 m / 98.4 ft due to the uncertainty of stratigraphic extrapolation) and ~ 640 m / 0.40 mi in the top unit Se (± 43 m / 141 ft due to the uncertainty of stratigraphic extrapolation) (see the right side chart in **Fig. 5b**). Similarly to S3, the throw of the main thrust fault decreases upward, which conforms with the geometry of a fault propagation fold with some strain accounted for by folding and overturning. That is, in the hanging-wall, next to the main fault $\mathbf{f_1}$, the strata are sub-horizontal or gently NE-dipping, whereas in the footwall next to $\mathbf{f_1}$ the strata are vertical or even overturned adjacent to the $\mathbf{f_1}$ and change to be gently SW-dipping.

4.3. Plan View Geometry

The cross-sections that have just been presented reveal a main thrust fault ($\mathbf{f_1}$) that is steeply dipping with an angle of between 60°SW and 70° SW. Structural mapping of the area (**Fig. 6**) confirms that it is a continuous fault between the two sections and that it extends for ~ 10 km / 6.21 mi along the length of the Lenghu5 fold-thrust belt. In addition to $\mathbf{f_1}$ several small splay faults are identified in the high resolution outcrop-mapping, which are equivalent to the second order structures described in the sections above. The main thrust fault $\mathbf{f_1}$ accounts for the majority (85 - 90%) of the deformation of the fault zone; while several splays of the main thrust fault are also observed in the field, either in the footwall or hanging-wall. The splay faults are not pervasively developed along the whole fault zone of the Lenghu5 fold-thrust belt, but are mostly located in the saddle between the two anticlines (**Fig. 6**). This implies that there is more distributed strain in the saddle because of the nonuniform deformation and strain accommodation during the propogration of the two anticlines and faults into this domain. The splay faults generate a number of fault lenses in both the hanging-wall and the footwall to the main fault. Approximately

80% of the second-order structures (e.g., the minor normal faults in the hanging-wall) occur in the fault zone and the hanging-wall, suggesting the largest strain in the hanging-wall and the central fault zone (**Fig. 6**). These normal faults terminate against the main thrust fault zone, with no continuation into the footwall, indicating they are faults developed; a) during the main thrust faulting and help accommodate the overall strain in the hanging-wall; and/or b) are in part associated with the interference of the propagating anticlines into the saddle area. The minor faults in the hanging-wall mostly concentrate in the fold cores and the density of the normal faults decreases away from the main thrust fault zone, emphasizing the role of these structures as accommodation features to the main fault.

From the structural map, we have constructed a series of additional sections across the fault zone to constrain the variation in structure along Lenghu5 (see the sections on the right side of **Fig. 6**). These sections reveal the general form of the strain accommodation and show that nonuniform thrust faulting dominates the structural lateral changes along the Lenghu5 fold-thrust belt, e.g., (i). the main thrust fault zone ($\mathbf{f_1}$) reaches local throw-maxima at two locations corresponding to the two structural culminations, forming the northern and southern anticlines in the hanging-wall; (ii). the main thrust fault zone ($\mathbf{f_1}$) beneath the southern anticline shows a maximum fault throw of ~ 840 m / 0.52 mi, which is approximately two times greater than indicated in the northern anticline (maximum throw of ~ 415 m / 0.26 mi); (iii). the saddle between the two anticlines has the lowest fault throw on the main fault, is where the fault throw changes rapidly and small scale structures (faults or folds) are preferentially developed. These observations are compatible with the saddle area being a possible stress-concentration area with rapidly increasing throw both northward and southward. These observations also indicate that the saddle area is one where the increased structural complexity is located where the interference between propagating folds and fault tips has occurred.

5. 3D Fault Architecture

5.1. Spatial Distribution of Fault Throw

The spatial distribution of fault throw is vital to the understanding of its association with the geometry of hanging-wall anticline and lateral variation of fault zone architecture. The stratigraphic boundaries were extrapolated above the present topography to predict the thrust fault cut-off position, which are used to estimate the throw across the fault zone. Here we also considered the possible impact of the uncertainties of fault zone throw associated with different stratigraphic extrapolation during the section construction (**Tab. 1**). In **Fig. 7a**, the splay fault $\mathbf{f_2}$ is exposed at the surface while the splay fault $\mathbf{f_3}$ is the blind splay that may account for the development of the minor folds in the southern footwall. A collation of the estimated fault zone throws along the structure for each cross section created is shown in the Throw-Distance chart (**Fig. 7b**). The throws are estimates at outcrop ground level. The Throw-Distance chart highlights the nonuniform deformation by faulting along the fault zone of Lenghu5. **Fig. 7b** highlights that the splay faults $\mathbf{f_2}$ and $\mathbf{f_3}$ present maximum fault zone throws of ~ 40 m / 130 ft (at section S6) and ~ 170 m / 0.11 mi (at section S9), respectively; while the main thrust fault zone $\mathbf{f_1}$ presents fault throw varying from ~ 300 m / 0.19 mi (minima at section S5) to ~ 680 m / 0.42 mi (maxima at section S9). The cumulative fault throw along the Lenghu5 thrust fault zone has also been calculated, ranging from ~330 m / 0.21 mi (minima at section S4) to ~860 m / 0.53 mi (maxima at section S9). The cumulative fault zone throw curve shows positions of highs and lows similar to that of the main thrust fault $\mathbf{f_1}$; there are also similar trends for the transition between the highs and lows. This indicates that the main thrust fault zone $\mathbf{f_1}$ accommodates the primary strain of the Lenghu5, while the splay faults (e.g., $\mathbf{f_2}$ and $\mathbf{f_3}$) generate the second order structures (e.g., minor folds). The two highs in the Throw-Distance chart represent the areas where the two anticlines have maximum heights (at section S3 and S9), while the middle low corresponds to the saddle between the two anticlines where the cumulative throw decreases rapidly to ~ 330 m / 0.21 mi (between sections S4 and S5). The shape of the Throw-Distance curves suggests a larger strain accommodation in the southern anticline compared to the northern anticline. This concurs with the more exposure of the older stratigraphic units in the southern anticline. The rapid decrease of fault throw in the southern end of the Lenghu5 fold-thrust belt suggests a SE-plunge of the Lenghu5 anticline towards a fault tip.

5.2. Lateral Variation of Fault Architecture

Integrating the detailed stratigraphy (**Fig. 2**), satellite image interpretation (**Fig. 3**), fault system maps (**Fig. 6**) and high-resolution sections (**Fig. 7**), allows us to consider the three-dimensional structural variation of the Lenghu5 fold-thrust belt (**Fig. 8**). The stratigraphic correlation between the hanging-wall and footwall supports the observation that the overall structure is dominated by a gentle southeast plunge. The 3D models demonstrate that both the hanging-wall anticlines and the fault zone show lateral variability from NW to SE. The Lenghu5 fault zone presents nonuniform combinations of a single-plane thrust fault and multiple splay faults as well as variable rotational, fold related straining. The changing fault array along the structure from northwest to southeast includes: (a) a main thrust only, (b) main thrust + one footwall splay, (c) main thrust + two footwall splays, (d) main thrust + a blind footwall splay and (e) main thrust + a hanging-wall splay (**Fig. 6** and **Fig. 8**). Furthermore, the hanging-wall anticlines are not continuous along the fault zone, but are linked by the saddle where the structural elevation is relatively low. The splay faults and normal faults are concentrated in the saddle between the northern and southern anticline, which implies the saddle has a more complex strain distribution. This suggests the possibility that two separate folds evolved and interacted during the structural history. The two topographic culminations (pink stratigraphy at the surface) correspond to the crestal highs of the two anticlines shown in sections S3 and S9 (**Fig. 5a, b**). As the two anticline highs are the sites with the maximum deformation in the Lenghu5 fold-thrust belt, the second-order accommodation faults (i.e., the normal faults in the hanging-wall) are expected also concentrated in the anticline areas close to the high cumulative throws.

5.3. Missed Strain at a Smaller Scale

A set of well-exposed outcrops (approximate section size 50 m / 164 ft × 30 m / 98.4 ft) in the Lenghu5 field enabled us to investigate how the structures we have presented on the cross-sections, at the > 100 m / 328 ft scale, are manifested at a scale < 100 m / 328 ft. Three well-exposed outcrops of the main thrust fault zones were mapped in detail (**Fig. 9**) to allow the generation of sections TF1, TF2 and TF3 (see positions in **Fig. 8c**). These three faults cut through the hanging-wall of the main thrust fault ($\mathbf{f_1}$) ~ 50m / 164 ft apart and are orientated sub-parallel with each other in a NW-SE direction. The fault geometry derived from these three outcrops represents fault zone cores and damage zones of the main thrust fault ($\mathbf{f_1}$), shown in the regional cross-sections in 3D models of **Fig. 8**, but reveals an order of magnitude more detail in the fault zone architecture close to the section S9.

The detailed architecture comprises an anticline with a flat crest against the thrust fault in the hanging-wall (see arrows in the SW side of the outcrops, **Fig. 9**). Although the hanging-wall anticline absorbs shortening, the overall strain is apparently dominated by faulting deformation and high shearing. The steeply dipping fault zone has sheared stratigraphic units comprising foliated fault rocks (primarily shales and subordinate sandstones), that account for the majority of the fault zone deformation (central portion of the outcrops). The shales have vertical dips and are smeared into the fault zone from the hanging-wall stratigraphy, while the sandstones are faulted and thinned by brittle deformation. Although the central fault domains are vertical, the bedding cannot be identified within the central fault zones, because intense deformation has destroyed the original bedding by smearing and faulting. The shearing into high strain fault zones generates clay smears and disrupted sand inclusions. Compared with the regional cross sections, these minor structural features observed in field are not observed at either the meso-scale or seismic scale.

6. Sub-surface Equivalent - Application to Exploration in DWFTBs

The preclusion of small structures (i.e., folds and fault arrays below seismic resolution) in the interpretation of seismic sections inhibits the understanding of the complexity of fold-thrust belts (e.g., Higgins et al., 2009; Iacopini et al., 2012). To evaluate the importance of these small scale structures we compare our field observations with a directly comparable sub-surface example. The Deep Water Fold-Thrust Belt (DWFTB) within the Niger Delta (e.g., Kostenko et al., 2008), has geometrically analogou structures to the Lenghu5 fold-thrust belt. An evaluation of the parameters needed to creat acceptable trishear models of the Lenghu5 and the DWFTB structures requires similar values. In detail, the cutoffs in the DWFTB 850 /840 sands and structural geometry requires trishear parameters represented by an apical angle of ~ 60°, a propagation/slip ratio of 2.0 – 2.5, and upward-steepening fault dips of 0°- 65° (see details in Kostenko et al., 2008), which are highly comparable to the parameters needed for the Lenghu5 fold-thrust belt (50°, 2.0, and 5°-60°, respectively) (see details in Pei et al., 2017b). Therefore, our field observations provides us with an opportunity to consider how much sub-seismic deformation is not imaged in sub-surface examples (**Fig. 10**). A seismic time slice (**Fig. 10a**) through a single structure in the DWTFB reveals two anticlinal folds in the hanging-wall above a NE-directing thrust fault zone, with smaller-scale normal faults developed in the hanging-wall and syncline in the adjacent footwall. As these faults are close to seismic resolution it is difficult to predict how many of these second order structures are just imaged in seismic sections. In section view (section A-A’ in **Fig. 10b**), the structure consists of an anticline and its underlying fault zone. Beneath the hanging-wall anticline, a NE-directing thrust fault is present and has a triangular fault zone domain bounded by two thrust faults. The triangular fault zone domain architecture has significant uncertainty in the interpreration because of the poor seismic imaging. As these frontal fold limbs of these structures are often exploration targets, reducing this geometric uncertainty and defining the possible fault architecture is critical for predicting prospectivity (Kostenko et al., 2008) .

When we compare the Niger delta example (**Fig. 11a**) with the Lenghu5 fold-thrust belt (**Fig. 11b**), there is a remarkable geometrical similarity. Along-axis anticlines are developed in the hanging-walls above the underlying thrust faults in both the Niger Delta example and the Lenghu5 fold-thrust belt. The small scale structures, i.e., folds and normal faults in the hanging-walls, visible in both the Lenghu5 fold-thrust belt and the Niger Delta example, are mostly developed surrounding the positions that show a high degree of lateral structural variation. This can be attributed to the development of small scale structures that accommodate the local stress field generated by the complexities of strain evolution at the intersection of deformation domains with lateral structural variations. The high degree of accordance between the Lenghu5 fold-thrust belt and the Niger Delta example suggests similar structural geometry may be developed in both surface outcrops and subsurface examples. However, in most previous studies in such a similar geological settings, the triangle domain with poor reflection in the seismic data has been simply interpreted as a fault zone that is likely to be composed of fault gouge, fault lenses and fault breccias (e.g., Corredor et al., 2005; Camerlo and Benson, 2006; Benesh et al., 2014).

Based on the high-resolution field observations, the dip trend variation in the three sections of the fault zone are used to depict the detailed fault architecture of the main thrust fault (**f_1**) (**Fig. 9** and **Fig. 12a, b**). As the three sections (**Fig. 9**) contain high strain deformation, it is necessary to exclude the dip measurements of the highly sheared bands or smearing gouges, in order to reflect the structural geometry within the steeply dipping fault zones, and to compare these to the dip panel elements in the poorly imaged triangle domain of the seismic section. The outcrop measured dip variation pattern demonstrates that the triangle domain between the thrust faults can be dominated by rotated dip panals rather than inhomogeneous fault breccia and fault gouges. The dip variation in the seismic section of the Niger Delta example is also interpreted based on the seismic reflection. Although the seismic bedding dip variation can explain the primary geometry (**Fig. 12c**), the triangle domain between the thrust faults cannot be properly interpreted, as the very detailed internal structural features are not resolvable in seismic sections. Our high resolution field observations from the Lenghu5 fold-thrust belt validate the possible presence of smaller scale structures and therefore suggest that there may be complex arrays of normal and reverse faults that are not seismically resolvable within the triangle domain. Although more examples of fault zone architecture are needed to enhance prediction, the study reported does demonstrate the value of integrating detailed outcrop and seismic analysis.

In the study of the Niger Delta Alpha-1X and Alpha-1ST1 wells (**Fig. 13**), which as we have demonstrated is a geometrically comparable structure to that in **Fig. 12c**, Kostenko et al. (2008) provided an elegant solution of the fold-fault geometry using a trishear algorithm (e.g., Erslev, 1991; Hardy and Ford, 1997) with a series of fault splays in the frontal limb. The discovery well Shell Alpha-1X was drilled vertically in the southeast part of the Alpha structure, while the deviated side-track well Alpha-1ST1 penetrated both the hanging-wall and the apparent footwall of the structure below the poor-seismic-image triangle zone between the previously interpreted thrust faults. By comparing the gamma-ray log signature of the Alpha-1X and Alpha-1ST1 wells, the fining-direction of the sandstones in the frontal limb was established to assist the detailed interpretation of the poor-seismic-image triangle zone. The poor-seismic-image zone had previously been interpreted as a fault zone comprising probably fault gauges, fault lenses and fault breccias. However, the

Alpha-1ST1 well penetrated the forelimb of the fold and revealed high angle dips in the poor-seismic-image zone (**Fig. 13b, c**), suggesting vertical or even overturned bedding rather than a simple fault zone. The results revealed the nature of the poorly imaged seismic zone and significantly improves the understanding of the prospect and the petroleum system in general. The predicted fault geometry by Kostenko et al. (2008), particularly within the poor-seismic-image triangle zone, is entirely consistent with the geometry that we observed in field in the Lenghu5 fold-thrust belt. Furthermore, the dip data for the Alpha-1X and Alpha-1ST1 boreholes that penetrate the frontal limb and footwall is consistent with the dip variations presented in our high resolution field observations (**Fig. 12b**).

Care must be taken when comparing field observations with sub-surface examples, in particular across different tectonic settings, deformation/burial/uplift history and fluid pressure evolution. Although the Lengh5 fold-thrust belt and the Niger Delta clearly have different geohistories, the magnitude of deformation, the gross geometry of the underlying controlling fault and heterogeneous stratigraphy through which the thrust faults propagate are broadly comparable. The resemblance in plan-view and cross-section geometry and indeed dip variations within the well data provides justification to tentatively use the sub-seismic observations in our study and apply them to the Niger Delta.

These findings are critical to minimise risk in petroleum exploration, particularly in the frontal limb of a thrust fault. However, these small scale structural features are obviously below seismic resolution, which results in limited imaging in a fold-thrust belt, particularly within a triangle zone between the main thrust fault and a splay. Without the aid of high resolution dip measurements from a borehole, it is difficult to make reliable interpretation of this no-seismic-image zone. As the field examples can provide realistic small scale geometry that can be expected in areas of low imaging quality, the high resolution outcrop studies can be an effective method to help improve the quality of subsurface seismic interpretation.

7. Discussion

7.1. Control of Fault Throw on Lateral Structural Variation

As demonstrated in **Fig. 2**, although folding deformation contributes to the regional section shortening in the Lenghu5 fold-thrust belt (e.g., ~ 33% at regional scale and ~ 20% at meso-scale), the overall strain is dominated by faulting deformation (e.g., ~ 67% at regional scale and ~ 80% at meso-scale). This study, focused on the meso-scale structural deformation at the surface and the shallow subsurface, has investigated the fault throw distribution and its links to structural variation along strike.

In previous studies, axial-trace maps were used to investigate the 3D geometry and lateral variation of natural structures (e.g., Shaw et al., 1994, 1996; Shaw and Suppe, 1996; Stone, 1996; Rowan and Linares, 2000; Hubert-Ferrari et al., 2007; Morley, 2009b). Structural trend analysis of the Medina Anticline (Eastern Cordillera, Colombia) (Shaw et al., 1994; Rowan and Linares, 2000) demonstrated that changes of fault throw along strike increases the lateral variation of the fault-related folding. In the study of a DWFTB in NW Borneo, Morley (2009a) identified that the density of hanging-wall normal faults increases where the throw rapidly changes along the fault zone. Lewis et al. (2009) quantitatively investigated the along-strike throw variation of the Pajarito fault system (Rio Grande rift, New Mexico), in which the saw-toothed throw-distance profiles indicate the association of fault throw changes with the structural variation along strike of the Pajarito fault system. Furthermore, as observed in the Lenghu5 fold-thrust belt, the degree of lateral structural variation is not always uniform but changes along the strike, which is probably related to the gradient of throw changes along the central fault zone. This observation is consistent with the studies of Morley (2009a) and Lewis et al. (2009). The similar triangle zone developed in the Niger Delta example (e.g., Kostenko et al., 2008) presents structural features that are highly comparable with that observed in the Lenghu5 fold-thrust belt. In both the two natural examples, the high degree lateral structural variations are all located in the positions where the fault throw changes rapidly between peaks and valleys in the throw vs distance curves.

In this research, our fault throw calculations reveals a similar throw variation along the Lenghu5 fold-thrust belt. The sections and structural models, presented for the Lenghu5 fold-thrust belt, particularly the central fault zone, illustrate a high degree of lateral structural variation, both in respect of fault architecture and fold geometry. As the southern portion shows a fault zone throw that is approximately two times larger than the northern portion, the high degree of lateral structural variation presented in the Lenghu5 fold-thrust belt corresponds to the nonuniform fault throw along strike, which is in good agreement with previous studies where structural geometry is related to the fault throw distribution (e.g., Shaw et al., 1994; Rowan and Linares, 2000; Kostenko et al., 2008).

There are two models of the structural evolution that might account for the links between the fault throw and the lateral strain accommodation at Lenghu5. The first is that the two folds develop from lateral variations in the fault displacement on an existing fault. The anticline culminations are then associated with the high displacement domains. The second model for the lateral strain variation at Lenghu5 is that two separate folds initially developed ahead of an irregular propagating thrust fault tip line as it propagated up section. In this case, the anticline culminations represent higher strain domains where the structurally higher deformation front, folds and then thrust faults propagated laterally out from. The central saddle area of the Lenghu5 folds may then represent a more complex strain zone associated with the interference during the propagation of the folds and faults.

7.2. Controls on Fault Splays and Small Scale Structures: Influence of Stratigraphy

In the previous section we considered the regional scale structural variation, but we also noticed that there is significant variation in minor fault presence and geometry that appears to have been influenced by the stratigraphy. The effects of stratigraphy on fault architecture has been widely discussed and it is commonly agreed that competent stratigraphy is strong and behaves in a brittle fashion while weaker stratigraphy inclines to ductile deformation (e.g., Corbett et al., 1987; Couzens and Wiltschko, 1996; Wilkins and Gross, 2002; Hardy and Finch, 2007; Simpson, 2009; Ferrill et al., 2014; Ferrill et al., 2017a; Ferrill et al., 2017b). Loveless et al. (2011) also suggested that stratigraphy heterogeneity determines the detailed fault architecture at meso-scale and micro-scale. The role of vertical mechanical heterogeneity on fault zone architecture development was highlighted by Davies et al. (2012). Our high resolution fieldwork demonstrated that the stratigraphy plays an important role in controlling the geometry of second-order structures, e.g., small fault splays with throw ranging from centimeters to tens of meters. In the Lenghu5 structure, the displacements decrease upward in the regional sections S3 and S9. Specifically, the fault displacement decreases when the fault propagates into the clay-rich units (e.g. Sb and Sd, **Fig. 5**). This can be attributed to the clay-rich units (e.g., Sb and Sd with low competency) that tend to experience ductile deformation and present lower fault propagation/slip ratios (Hardy and Ford, 1997; Pei et al., 2015), which contributes to the upward decreasing displacement when a fault propagates from a sandy unit into a clay-rich unit. In plan view, the small fault splays also present decreasing throws or die out when they propagate into the clay-rich units Sb and Sd, because the ductile deformation can be accommodated through bedding parallel flexural slip rather than brittle fault deformation (e.g., Jamison, 1987; Erslev, 1991). Moreover, within the central main thrust fault zone (**Fig. 6, Fig. 9**), the splay faults and fault lenses are developed in the footwall where the high heterogeneity package Sd is truncated by the fault zone; in contrast, only a single reverse fault is developed where the low heterogeneity package Sb and Sc are truncated in the northern end. Therefore, it is inferred that the fault zone presents a minimal complexity when the faults cut a sequence with low mechanical heterogeneity, while a greater complexity of fault zones is formed when the faults cut a sequence with high mechanical heterogeneity. This observation is in agreement with the previous studies focusing on fault architecture in multi-layered sequences (e.g., Peacock and Sanderson, 1992; McGrath and Davison, 1995; Childs et al., 1996a; Schöpfer et al., 2006; Welch et al., 2009; Ferrill et al., 2014; Ferrill et al., 2017a; Ferrill et al., 2017b). In the sub-surface equivalent example from the Niger Delta (**Fig. 12c**), with detailed stratigraphic constraints established, the outcrop studies help to constrain the range of possibilities in fault zones and the nature of fold or fault splays developed in the areas with limited seismic imaging (e.g., the steep dips in the forelimb of an anticline).

7.3. Scale-dependant Effects of Fault Throw and Stratigraphy

As discussed above, both fault throw and stratigraphy play impacts on the resultant structural geometry and fault zone architecture. However, these two important parameters scale-dependant. In the Lenghu5 fold-thrust belt, the primary structural geometry (i.e., the two anticlines at regional scale) is clearly associated with the lateral variations in cumulative strain and fault throw (**Fig. 12a**), whereas the minor structural geometry (i.e., the small fault splays in the hanging-wall at meso-scale) is likely determined by the stratigraphy (**Fig. 12b**). The seismic example from the Niger Delta (**Fig. 12c**) also demonstrates that the overall geometry of a structure is dominated by the regional strain and fault throw, whereas the small scale deformation features (e.g., the central fault zone) are more likely to be controlled by the local stratigraphy (e.g., Kostenko et al., 2008). This is probably because fault throws normally show important lateral variation at the regional scale (> 1km / 0.62 mi), whereas stratigraphy shows heterogeneity at a much smaller scale, e.g., meso-scale (10-100m / 32.8 – 328 ft). This is compatible with the established concept that the fault throw network controls the regional strain, , whereas the stratigraphy can affect the deformation features at smaller scale, i.e., meso-scale. This indicates that the important parameters (e.g., fault throw and stratigraphy) on structural geometry is scale-dependant, which highlights that different controlling parameters should be taken into account when evaluating the fault architecture and structural geometry at different scales.

8. Conclusion

By integrating field observations and analyses of the Lenghu5 fold-thrust belt and an example of structures in the DWFTB Niger Delta, we conclude that:

(1). At both regional and meso-scale, the overall strain in the Lenghu5 fold-thrust belt is dominated by faulting deformation (67% - 80%), although folding deformation absorbs section shortening as well (20% - 33%).

(2). The main thrust fault zone accounts for 80% - 85% of the total throw, which is sufficient to be well-imaged on a seismic profile, while the smaller scale folds and splay faults account for 15% - 20% of the throw that is beyond seismic resolution.

(3). The high degree of lateral variation in strain distribution along the structure, as observed from plan view structural mapping, is associated with laterally varying fault throw.

(4). Although at a regional scale (> 1km / 0.62 mi) strain is accommodated by a single through going fault zone, the local stratigraphy is likely to impact on how strain is accommodated at a smaller scale (10m -100m / 32.8 – 328 ft);.in stratigraphy that is dominated by mechanically strong units, e.g. clastics, single faults dominate, whereas strain in heterolithic units is dominated by multiple-fault splays or folding.

(5). The fault architecture models at outcrop scale can be used to help predict the detailed structural styles and strain within a fold-thrust belt that is beyond the resolution of seismic surveys, because of either insufficient fault throw or high-angle bedding that are difficult to be imaged on seismic profile.

References Cited

Alcalde, J., C. E. Bond, G. Johnson, J. F. Ellis, and R. W. Butler, 2017, Impact of seismic image quality on fault interpretation uncertainty: GSA Today, v. 27, p. 4-10.

Allen, M. B., and S. J. Vincent, 1997, Fault reactivation in the Junggar region, northwest China: the role of basement structures during Mesozoic-Cenozoic compression: Journal of the Geological Society, v. 154, p. 151-155.

Alves, T. M., and C. Elliott, 2014, Fluid flow during early compartmentalisation of rafts: A North Sea analogue for divergent continental margins: Tectonophysics, v. 634, p. 91-96.

Bally, A. W., P. Gordy, and G. A. Stewart, 1966, Structure, seismic data, and orogenic evolution of southern Canadian Rocky Mountains: Bulletin of Canadian Petroleum Geology, v. 14, p. 337-381.

Barclay, J., and D. G. Smith, 1992, Western Canada foreland basin oil and gas plays: in R.W. Macqueen and D.A. Leckie, eds., Foreland Basins and Fold Belts: American Association of Petroleum Geologists Memoir, v. 55, p. 191-228.

Benesh, N. P., A. Plesch, and J. H. Shaw, 2014, Geometry, kinematics, and displacement characteristics of tear-fault systems: An example from the deep-water Niger Delta: American Association of Petroleum Geologists Bulletin, v. 98, p. 465-482.

Brandes, C., and D. C. Tanner, 2014, Fault-related folding: A review of kinematic models and their application: Earth-Science Reviews, v. 138, p. 352-370.

Burchfiel, B. C., Q. Deng, P. Molnar, L. Royden, Y. Wang, P. Zhang, and W. Zhang, 1989, Intracrustal detachment within zones of continental deformation: Geology, v. 17, p. 748-752.

Caine, J. S., J. P. Evans, and C. B. Forster, 1996, Fault zone architecture and permeability structure: Geology, v. 24, p. 1025-1028.

Camerlo, R. H., and E. F. Benson, 2006, Geometric and seismic interpretation of the Perdido fold belt: Northwestern deep-water Gulf of Mexico: American Association of Petroleum Geologists Bulletin, v. 90, p. 363-386.

Chen, Z. Y., L. Q. Wang, S. P. Chen, and Z. X. Wang, 2005, Tectonic model and its deformation feature of Cenozoic in west section of Lenghu structural belt, northern margin of Qaidam basin (in Chinese with English abstract): Xinjiang Petroleum Geology, v. 26, p. 614-617.

Childs, C., T. Manzocchi, J. J. Walsh, C. G. Bonson, A. Nicol, and M. P. J. Schöpfer, 2009, A geometric model of fault zone and fault rock thickness variations: Journal of Structural Geology, v. 31, p. 117-127.

Childs, C., A. Nicol, J. J. Walsh, and J. Watterson, 1996a, Growth of vertically segmented normal faults: Journal of Structural Geology, v. 18, p. 1389-1397.

Childs, C., J. J. Walsh, T. Manzocchi, J. Strand, A. Nicol, M. Tomasso, M. P. J. Schöpfer, and A. C. Aplin, 2007, Definition of a fault permeability predictor from outcrop studies of a faulted turbidite sequence, Taranaki, New Zealand: Geological Society of London Special Publications, v. 292, p. 235-258.

Childs, C., J. Watterson, and J. J. Walsh, 1996b, A model for the structure and development of fault zones: Journal of the Geological Society, v. 153, p. 337-340.

Corbett, K., M. Friedman, and J. Spang, 1987, Fracture development and mechanical stratigraphy of Austin Chalk, Texas: American Association of Petroleum Geologists Bulletin, v. 71, p. 17-28.

Corredor, F., J. H. Shaw, and F. Bilotti, 2005, Structural styles in the deep-water fold and thrust belts of the Niger Delta: American Association of Petroleum Geologists Bulletin, v. 89, p. 753-780.

Couzens, B. A., and D. V. Wiltschko, 1996, The control of mechanical stratigraphy on the formation of triangle zones: Bulletin of Canadian Petroleum Geology, v. 44, p. 165-179.

Coward, M. P., 1983a, The thrust and shear zones of the Moine thrust zone and the NW Scottish Caledonides: Journal of the Geological Society, v. 140, p. 795-811.

Coward, M. P., 1983b, Thrust tectonics, thin skinned or thick skinned, and the continuation of thrusts to deep in the crust: Journal of Structural Geology, v. 5, p. 113-123.

Cowgill, E., A. Yin, W. X. Feng, and Z. Qing, 2000, Is the North Altyn fault part of a strike-slip duplex along the Altyn Tagh fault system?: Geology, v. 28, p. 255-258.

Cowie, P. A., R. J. Knipe, and I. G. Main, 1996, Introduction to the Special Issue: Scaling Laws for fault and fracture populations - analyses and applications: Journal of Structural Geology, v. 18, p. v-xi.

Cowie, P. A., and C. H. Scholz, 1992, Displacement-length scaling relationship for faults: data synthesis and discussion: Journal of Structural Geology, v. 14, p. 1149-1156.

Cowie, P. A., C. Vanneste, and D. Sornette, 1993, Statistical physics model for the spatiotemporal evolution of faults: Journal of Geophysical Research, v. 98, p. 21809-21821.

Davies, R. K., R. J. Knipe, and M. J. Welch, 2012, The role of vertical mechanical heterogeneity in predicting fault zone architecture: 3rd EAGE International Conference on Fault and Top Seals.

Egan, S. S., T. S. Buddin, S. J. Kane, and G. D. Williams, 1997, Three-dimensional modelling and visualisation in structural geology: New techniques for the restoration and balancing of volumes: Proceedings of the 1996 Geoscience Information Group Conference on Geological Visualisation. Electronic Geology Special Volume, v. 1, p. 67-82.

Erslev, E. A., 1991, Trishear Fault-Propagation Folding: Geology, v. 19, p. 617-620.

Ferrill, D. A., M. A. Evans, R. N. McGinnis, A. P. Morris, K. J. Smart, S. S. Wigginton, K. D. H. Gulliver, D. Lehrmann, E. de Zoeten, and Z. Sickmann, 2017a, Fault zone processes in mechanically layered mudrock and chalk: Journal of Structural Geology, v. 97, p. 118-143.

Ferrill, D. A., R. N. McGinnis, A. P. Morris, K. J. Smart, Z. T. Sickmann, M. Bentz, D. Lehrmann, and M. A. Evans, 2014, Control of mechanical stratigraphy on bed-restricted jointing and normal faulting: Eagle Ford Formation, south-central Texas: American Association of Petroleum Geologists Bulletin, v. 98, p. 2477-2506.

Ferrill, D. A., A. P. Morris, R. N. McGinnis, K. J. Smart, S. S. Wigginton, and N. J. Hill, 2017b, Mechanical stratigraphy and normal faulting: Journal of Structural Geology, v. 94, p. 275-302.

Fokker, P. A., K. Visser, E. Peters, G. Kunakbayeva, and A. G. Muntendam-Bos, 2012, Inversion of surface subsidence data to quantify reservoir compartmentalization: A field study: Journal of Petroleum Science and Engineering, v. 96–97, p. 10-21.

Fossen, H., and A. Rotevatn, 2016, Fault linkage and relay structures in extensional settings—A review: Earth-Science Reviews, v. 154, p. 14-28.

Hardy, S., and E. Finch, 2007, Mechanical stratigraphy and the transition from trishear to kink-band fault-propagation fold forms above blind basement thrust faults: A discrete-element study: Marine and Petroleum Geology, v. 24, p. 75-90.

Hardy, S., and M. Ford, 1997, Numerical modeling of trishear fault propagation folding: Tectonics, v. 16, p. 841-854.

Higgins, S., B. Clarke, R. J. Davies, and J. Cartwright, 2009, Internal geometry and growth history of a thrust-related anticline in a deep water fold belt: Journal of Structural Geology, v. 31, p. 1597-1611.

Hubert-Ferrari, A., J. Suppe, R. Gonzalez-Mieres, and X. Wang, 2007, Mechanisms of active folding of the landscape (southern Tian Shan, China): Journal of Geophysical Research: Solid Earth, v. 112, B03S09.

Iacopini, D., R. Butler, and S. Purves, 2012, Seismic imaging of thrust faults and structural damage: A visualization workflow for deepwater thrust belts: First Break, v. 30, p. 77-84.

Iacopini, D., and R. W. H. Butler, 2011, Imaging deformation in submarine thrust belts using seismic attributes: Earth and Planetary Science Letters, v. 302, p. 414-422.

Jamison, W. R., 1987, Geometric analysis of fold development in overthrust terranes: Journal of Structural Geology, v. 9, p. 207-219.

Jolivet, M., M. Brunel, D. Seward, Z. Xu, J. Yang, J. Malavieille, F. Roger, A. Leyreloup, N. Arnaud, and C. Wu, 2003, Neogene extension and volcanism in the Kunlun Fault Zone, northern Tibet: New constraints on the age of the Kunlun Fault: Tectonics, v. 22, p. 1-23.

Kane, S. J., G. D. Williams, T. S. Buddin, S. S. Egan, and D. Hodgetts, 1997, Flexural-slip based restoration in 3D, a new approach: 1997 AAPG Annual Convention Official Program A, v. 58.

Kolyukhin, D., S. Schueller, M. Espedal, and H. Fossen, 2010, Deformation band populations in fault damage zone—impact on fluid flow: Computational Geosciences, v. 14, p. 231-248.

Kostenko, O. V., S. J. Naruk, W. Hack, M. Poupon, H.-J. Meyer, M. Mora-Glukstad, C. Anowai, and M. Mordi, 2008, Structural evaluation of column-height controls at a toe-thrust discovery, deep-water Niger Delta: American Association of Petroleum Geologists Bulletin, v. 92, p. 1615-1638.

Lewis, C. J., J. N. Gardner, E. S. Schultz-Fellenz, A. Lavine, S. L. Reneau, and S. Olig, 2009, Fault interaction and along-strike variation in throw in the Pajarito fault system, Rio Grande rift, New Mexico: Geosphere, v. 5, p. 252-269.

Liu, D. L., X. M. Fang, J. P. Gao, Y. D. Wang, W. L. Zhang, Y. F. Miao, Y. Q. Liu, and Y. Z. Zhang, 2009, Cenozoic Stratigraphy Deformation History in the Central and Eastern of Qaidam Basin by the Balance Section Restoration and its Implication: Acta Geologica Sinica-English Edition, v. 83, p. 359-371.

Loveless, S., V. Bense, and J. Turner, 2011, Fault architecture and deformation processes within poorly lithified rift sediments, Central Greece: Journal of Structural Geology, v. 33, p. 1554-1568.

McGrath, A. G., and I. Davison, 1995, Damage zone geometry around fault tips: Journal of Structural Geology, v. 17, p. 1011-1024.

Meyer, B., P. Tapponnier, L. Bourjot, F. Metivier, Y. Gaudemer, G. Peltzer, G. Shunmin, and C. Zhitai, 1998, Crustal thickening in Gansu-Qinghai, lithospheric mantle subduction, and oblique, strike-slip controlled growth of the Tibet plateau: Geophysical Journal International, v. 135, p. 1-47.

Molnar, P., and P. Tapponnier, 1975, Cenozoic Tectonics of Asia - Effects of a Continental Collision: Science, v. 189, p. 419-426.

Morley, C., 2009a, Geometry of an oblique thrust fault zone in a deepwater fold belt from 3D seismic data: Journal of Structural Geology, v. 31, p. 1540-1555.

Morley, C. K., 2009b, Growth of folds in a deep-water setting: Geosphere, v. 5, p. 59-89.

Pang, X., Y. Li, and Z. Jiang, 2004, Key geological controls on migration and accumulation for hydrocarbons derived from mature source rocks in Qaidam Basin: Journal of Petroleum Science and Engineering, v. 41, p. 79-95.

Paton, D., M. Carr, B. Trudgill, H. Ortner, and D. A. Medwedeff, 2007, Alpine-scale 3D geospatial modeling: Applying new techniques to old problems: Geosphere, v. 3, p. 527-549.

Peacock, D. C. P., and D. J. Sanderson, 1991, Displacements, segment linkage and relay ramps in normal fault zones: Journal of Structural Geology, v. 13, p. 721-733.

Peacock, D. C. P., and D. J. Sanderson, 1992, Effects of layering and anisotropy on fault geometry: Journal of the Geological Society, v. 149, p. 793-802.

Peacock, D. C. P., and D. J. Sanderson, 1994, Geometry and development of relay ramps in normal fault systems: American Association of Petroleum Geologists Bulletin, v. 78, p. 147-165.

Pei, Y., D. A. Paton, and R. J. Knipe, 2014, Defining a 3-dimensional trishear parameter space to understand the temporal evolution of fault propagation folds: Journal of Structural Geology, v. 66, p. 284-297.

Pei, Y., D. A. Paton, R. J. Knipe, and K. Wu, 2015, A review of fault sealing behaviour and its evaluation in siliciclastic rocks: Earth-Science Reviews, v. 150, p. 121-138.

Pei, Y., D. A. Paton, R. J. Knipe, and K. Wu, 2017a, Examining fault architecture and strain distribution using geospatial and geomechanical modelling: An example from the Qaidam basin, NE Tibet: Marine and Petroleum Geology, v. 84, p. 1-17.

Pei, Y., D. A. Paton, K. Wu, and L. Xie, 2017b, Subsurface structural interpretation by applying trishear algorithm: An example from the Lenghu5 fold-and-thrust belt, Qaidam Basin, Northern Tibetan Plateau: Journal of Asian Earth Sciences, v. 143, p. 343-353.

Place, J., Y. Géraud, M. Diraison, G. Herquel, J. B. Edel, M. Bano, E. Le Garzic, and B. Walter, 2016, Structural control of weathering processes within exhumed granitoids: Compartmentalisation of geophysical properties by faults and fractures: Journal of Structural Geology, v. 84, p. 102-119.

Price, R. A., 1981, The Cordilleran forelarid thrust and fold belt in the southern'Canadian Rocky Mountains: Geological Society of London Special Publications, v. 9, p. 427-448.

Roche, V., C. Homberg, and M. Rocher, 2012, Architecture and growth of normal fault zones in multilayer systems: A 3D field analysis in the South-Eastern Basin, France: Journal of Structural Geology, v. 37, p. 19-35.

Rotevatn, A., H. Fossen, J. Hesthammer, T. E. Aas, and J. A. Howell, 2007, Are relay ramps conduits for fluid flow? Structural analysis of a relay ramp in Arches National Park, Utah: Geological Society of London Special Publications, v. 270, p. 55-71.

Rowan, M. G., and R. Linares, 2000, Fold-evolution matrices and axial-surface analysis of fault-bend folds: application to the Medina Anticline, Eastern Cordillera, Colombia: American Association of Petroleum Geologists Bulletin, v. 84, p. 741-764.

Schöpfer, M. P. J., C. Childs, and J. J. Walsh, 2006, Localisation of normal faults in multilayer sequences: Journal of Structural Geology, v. 28, p. 816-833.

Shaw, J. H., S. C. Hook, and J. Suppe, 1994, Structural Trend Analysis by Axial Surface Mapping: American Association of Petroleum Geologists Bulletin, v. 78, p. 700-721.

Shaw, J. H., S. C. Hook, and J. Suppe, 1996, Structural trend analysis by axial surface mapping: Reply: American Association of Petroleum Geologists Bulletin, v. 80, p. 780-787.

Shaw, J. H., and J. Suppe, 1996, Earthquake hazards of active blind-thrust faults under the central Los Angeles basin, California: Journal of Geophysical Research-Solid Earth, v. 101, p. 8623-8642.

Simpson, G. D. H., 2009, Mechanical modelling of folding versus faulting in brittle–ductile wedges: Journal of Structural Geology, v. 31, p. 369-381.

Stone, D. S., 1996, Structural trend analysis by axial surface mapping: discussion: American Association of Petroleum Geologists Bulletin, v. 80, p. 770-779.

Suppe, J., and D. A. Medwedeff, 1990, Geometry and Kinematics of Fault-Propagation Folding: Eclogae Geologicae Helvetiae, v. 83, p. 409-454.

Tapponnier, P., B. Meyer, J. P. Avouac, G. Peltzer, Y. Gaudemer, S. M. Guo, H. F. Xiang, K. L. Yin, Z. T. Chen, S. H. Cai, and H. G. Dai, 1990, Active Thrusting and Folding in the Qilian-Shan, and Decoupling between Upper Crust and Mantle in Northeastern Tibet: Earth and Planetary Science Letters, v. 97, p. 382-403.

Torabi, A., and H. Fossen, 2009, Spatial variation of microstructure and petrophysical properties along deformation bands in reservoir sandstones: American Association of Petroleum Geologists Bulletin, v. 93, p. 919-938.

Wang, B. Q., Q. H. Wang, H. L. Chen, and A. C. Xiao, 2006a, Three-D mensional structure modeling and structural analysis of the lenghu area on the northern margin of Qaidam basin: Geotectonica et Metallogenia, v. 30, p. 430-434.

Wang, E., F. Y. Xu, J. X. Zhou, J. L. Wan, and B. C. Burchfiel, 2006b, Eastward migration of the Qaidam basin and its implications for Cenozoic evolution of the Altyn Tagh fault and associated river systems: Geological Society of America Bulletin, v. 118, p. 349-365.

Wang, E. C., and B. C. Burchfiel, 2004, Late cenozoic right-lateral movement along the Wenquan fault and associated deformation: Implications for the kinematic history of the Qaidam Basin Northeastern Tibetan Plateau: International Geology Review, v. 46, p. 861-879.

Watkins, H., R. W. H. Butler, and C. E. Bond, 2017, Using laterally compatible cross sections to infer fault growth and linkage models in foreland thrust belts: Journal of Structural Geology, v. 96, p. 102-117.

Welch, M. J., R. J. Knipe, C. Souque, and R. K. Davies, 2009, A Quadshear kinematic model for folding and clay smear development in fault zones: Tectonophysics, v. 471, p. 186-202.

Wilkins, S. J., and M. R. Gross, 2002, Normal fault growth in layered rocks at Split Mountain, Utah: influence of mechanical stratigraphy on dip linkage, fault restriction and fault scaling: Journal of Structural Geology, v. 24, p. 1413-1429.

Wu, L., A. Xiao, L. Wang, Z. Shen, S. Zhou, Y. Chen, L. Wang, D. Liu, and J. Guan, 2011, Late Jurassic–Early Cretaceous Northern Qaidam Basin, NW China: Implications for the earliest Cretaceous intracontinental tectonism: Cretaceous Research, v. 32, p. 552-564.

Xia, W. C., N. Zhang, X. P. Yuan, L. S. Fan, and B. S. Zhang, 2001, Cenozoic Qaidam basin, China: A stronger tectonic inversed, extensional rifted basin: American Association of Petroleum Geologists Bulletin, v. 85, p. 715-736.

Yang, Y. T., B. Ritts, C. N. Zou, T. G. Xu, B. M. Zhang, and P. Xi, 2003, Upper triassic-middle jurassic stratigraphy and sedimentology in the NE Qaidam Basin, NW China: Petroleum geological significance of new outcrop and subsurface data: Journal of Petroleum Geology, v. 26, p. 429-449.

Yin, A., Y. Dang, M. Zhang, M. W. McRivette, W. P. Burgess, and X. Chen, 2007, Cenozoic tectonic evolution of Qaidam basin and its surrounding regions (part 2): Wedge tectonics in southern Qaidam basin and the Eastern Kunlun Range: Geological Society of America Special Papers, v. 433, p. 369-390.

Yin, A., Y. Q. Dang, L. C. Wang, W. M. Jiang, S. P. Zhou, X. H. Chen, G. E. Gehrels, and M. W. McRivette, 2008a, Cenozoic tectonic evolution of Qaidam basin and its surrounding regions (Part 1): The southern Qilian Shan-Nan Shan thrust belt and northern Qaidam basin: Geological Society of America Bulletin, v. 120, p. 813-846.

Yin, A., Y. Q. Dang, M. Zhang, X. H. Chen, and M. W. McRivette, 2008b, Cenozoic tectonic evolution of the Qaidam basin and its surrounding regions (Part 3): Structural geology, sedimentation, and regional tectonic reconstruction: Geological Society of America Bulletin, v. 120, p. 847-876.

Zhou, J. X., F. Y. Xu, T. C. Wang, A. F. Cao, and C. M. Yin, 2006, Cenozoic deformation history of the Qaidam Basin, NW China: Results from cross-section restoration and implications for Qinghai-Tibet Plateau tectonics: Earth and Planetary Science Letters, v. 243, p. 195-210.

Zhu, L. D., C. S. Wang, H. B. Zheng, F. Xiang, H. S. Yi, and D. Z. Liu, 2006, Tectonic and sedimentary evolution of basins in the northeast of Qinghai-Tibet Plateau and their implication for the northward growth of the plateau: Palaeogeography, Palaeoclimatology, Palaeoecology, v. 241, p. 49-60.

Authors' Vitae

Yangwen Pei: China University of Petroleum, School of Geosciences, Qingdao 266580, China; Email: peiyangwen@upc.edu.cn

Yangwen Pei is an associate professor in the School of Geosciences of China University of Petroleum. He received his B.Sc. degree in geology from Zhejiang University, Hangzhou, China, in 2008, and Ph.D. degree in structural geology from University of Leeds, United Kingdom, in 2014. His current research focuses on structural geology in contractional geological settings, covering basin evolution, fault architecture, rock deformation, and fault sealing evaluation.

D. A. Paton: Basin Structure Group, Institute of Applied Geosciences, School of Earth and Environment, University of Leeds, Leeds, UK; Email: d.a.paton@leeds.ac.uk

Douglas Paton is Chair of Structural Geology and Basin Analysis at the University of Leeds. He obtained his Ph.D. from Edinburgh University. He has worked at the GFZ Potsdam and Chevron Center of Research Excellence at the Colorado School of Mines. He is a professor of basin analysis and structural geology at the University of Leeds, investigates rift and passive margin evolution through the Basin Structure Group, and is course director of the M.Sc. structural geology with geophysics.

R. J. Knipe: University of Leeds, School of Earth & Environment, Leeds LS2 9JT, England; Email: rjknipe100@hotmail.co.uk

Rob Knipe is emeritus professor of structural geology at University of Leeds. He has a distinguished career as a structural geologist investigating the mechanisms of deformation in rocks and has won awards from the Geological Society for his research. During the past 20 years he has focused his attention on faulting and fault sealing and the influence of deformation on fluid flow in rocks.

H. Lickorish: 22 140 Point Drive NW, Calgary T3D 4W3, Canada; Email: henry@henrylickorish.com

Henry Lickorish Henry graduated from Cambridge University (UK) in 1988 with a B.A. in Geological Sciences, and from the University of Calgary (Canada) in 1992 with a Ph.D. in Structural Geology, followed by post-doctoral research positions at the University of Leeds (UK), and ETH (Switzerland). He is now an independent geologist specializing at field-based fault zone evolution, fault architecture, mechanical stratigraphy, and structural modelling.

A. Li: Central Area Exploration Division, Saudi Aramco, Dhahran, 31311, Kingdom of Saudi Arabia; Email: anrenlilinzeng@aol.com

Anren Li received his BS.c. degree in Sedimentology from Chengdu University of Technology, China, in 1990, and Ph.D degree in Sedimentology & Petroleum from Victoria University of Wellington, New Zealand, in 1997. He had work for Rock Deformation Research (RDR) for 12 years focusing on the meso-scale fault architecture, micro- rock deformation, petrophysics, fault sealing evaluation. He had been a senior geologist in trap and seal characterization for Schlumberger Oilfield UK Plc from 2012 to 2015. He is currently working as a geology specialist at the Central Area Exploration Division of Saudi Aramco.

K. Wu: China University of Petroleum, School of Geosciences, Qingdao 266580, China; Email: wukongyou@upc.edu.cn

Kongyou Wu is a professor of Structural Geology at China University of Petroleum. He received his Ph.D. degree in Geology from China University of Petroleum in 2004. His current research focuses on basin modelling, fault-related folding, fault zone structure and, petroleum migration and accumulation.

Figure Captions

Figure 1 Structural map and cross sections of the Qaiam Basin and the Lenghu5 fold-thrust belt. (a): Structural interpretation of SRTM EDM data; (b): a NE-SW section through the central Qaidam Basin (modified from Yin et al., 2008b); (c): an interpreted seismic section across the Lenghu5 fold-thrust belt (modified from Pei et al., 2014), in which the blue rectangle represents the approximate coverage of sections constructed based on field geologic data. SRTM = Shuttle Radar Topography Mission. DEM = Digital Elevation Model.

Figure 2 Regional stratigraphy and stratigraphic correlation of the Lenghu5 fold-thrust belt. The regional stratigraphy has been recorded along three pathes: HW1 and HW2 in the hanging-wall (SW) and FW in the footwall (NE). The stratigraphic correlation between stratigraphic columns is used to estimate the fault throw between the hanging-wall and footwall (modified from Pei et al., 2017a). HW = hanging-wall. FW = footwall.

Figure 3 Satellite map showing the distribution of regional cross sections constructed based on high-resolution fieldwork. Ten parallel regional cross sections were constructed based on the field-measured stratigraphy (i.e., HW1, HW2, FW) and dip data. The grey stripes (e.g., NW-striking dash lines) presented in the satellite image are wind blown traces. Sections S3 and S9 are used to demonstrate the structural styles of the Lenghu5 fold-thrust belt (Fig. 5), while sections S1-S10 are used to analyse the spatial distrubtion of fault throw (Fig. 7).

Figure 4 Evaluation of contribution of faulting and folding deformation to the overall strain in the Lenghu5 fold-thrust belt. (a): present section; (b): fault throw restored; (c): unfolded layers. At regional scale, there are two components of the overall section shortening, which are ~ 1.03 km / 3.38 ft by faulting deformation and ~ 0.51 km / 1.67 ft by folding deformation; whereas at meso-scale, faulting and folding deformation accounted for section shortening (the green horizon bounded by the blue rectangle) of ~ 0.86 km / 2.82 ft and ~ 0.24 km / 0.79 ft, respectively.

Figure 5 Regional cross section S3 and S9 through the northern and southern anticlines (see position in Fig. 3) to demonstrate the subsurface structural geometry of the Lenghu5 fold-thrust belt. (a) Section 3: the fault zone consists of a main fault $\mathbf{f_1}$ with a throw of ~ 415m / 0.26 mi and a splay fault $\mathbf{f_2}$ that only presents a throw of ~ 50m / 164 ft. The main fault $\mathbf{f_1}$ does not maintain a constant fault throw up fault, but presents decreasing throw. (b) Section 9: the fault zone consists of a main fault $\mathbf{f_1}$ with a throw of ~ 834m / 0.52 mi and a blind splay fault $\mathbf{f_3}$ with a throw of only ~ 150m / 0.09 mi. Similarly with Section3, the main fault $\mathbf{f_1}$ does not keep a constant fault throw up fault, but presents decreasing throw. The uncertainty ranges of fault throw estimation are caused to different methods of stratigraphic extrapolation.

Figure 6 Structural map of the Lenghu5 fold-thrust belt based on the field data, including stratigraphy, dip, fault trace, etc. Both the primary structures and second order structures are all integrated. The right-side charts are schematic profiles to demonstrate the general geometry of the fault zone (without smaller normal faults presented at this scale), presenting high degree of lateral variation, particularly the fault zone architecture from northwest to southeast.

Figure 7 3D structural model of the Lenghu5 fold-thrust belt and the fault throw measurement with error bars along the Lenghu5 fault zone (see positions of sections S1-S10 in Fig. 3). F_{cum} represents cumulative fault throw of the Lenghu5 fault zone. The highs and lows in the fault throw curves correspond to the positions with high degree of lateral structural variation.

Figure 8 3D models integrating multi-scale structures to demonstrate the structural geometry and lateral variation of the Lenghu5 fold-thrust belt. The nonuniform fault throw along the fault zone leads to high degree of lateral structural variation. The primary structural style is determined by the main thrust fault, while the small-scale structures (e.g., small folds and faults) are developed as a result of the fault splays.

Figure 9 Detailed outcrop maps of TF1, TF2 and TF3 showing the latera structurall variation of the Lenghu5 thrust fault zone (see detailed position in Fig. 3 and Fig. 8c). These fault zone outcrops present similar structural geometries, however, lateral structural variation can be observed when focusing on smaller deformation features.

Figure 10 A DWFTB example from the Niger Delta (seismic data from VSA: Virtual Seismic Atlas). (a) A time slice (t=4400 ms) showing folds and fault arrays in plan view. (b) A seismic section showing fold and fault geometry, however, with uncertainty in the interpreted fault zone.

Figure 11 Comparison between the Lenghu5 fold-thrust belt and the Niger Delta seismic time slice (from VSA). The Niger Delta example presents hanging-wall geometry similar to the Lenghu5 fold-thrust belt, particularly the hanging-wall anticlines and minor faults. The good accordance between the two may suggest the potential prediction of small scale structures that are under seismic resolution, based on the lateral structural variation.

Figure 12 Comparison of fault architecture and structural geometry between the Lenghu5 fold-thrust belt (a, b) and a seismic example from the Niger Delta (c) (see the detailed dip variation along the throw in both b and c). The good correlation between the two demonstrate that the overall geometry of a structural is dominated by the fault throw, whereas the small scale deformation features (e.g., the internal features within the triangular fault domain) are more likely to be controlled by the local stratigraphy.

Figure 13 An example from the Niger Delta, presenting detailed structural geometry assisted by wells Alpha-1X and Alpha-1ST1 (modified from Kostenko et al., 2008). The dip variation of the frontal limb in the depth-converted seismic section indicates the complexity of structural geometry within the poor-seismic-image triangle zone, rather than a simple fault zone comprising of fault gouges, fault lenses and fault breccias.

Table Captions

Table 1 Statistics of fault throw estimation of the Lenghu5 thrust fault zone. Due to the different ways of stratigraphic extrapolation to estimate fault throw, there is uncertainty of the estimated fault throw. The fault throw curves were built using average value of the fault throw in each individual section, with an uncertainty range constrained by maximum and minimum values of the fault throw.

Figure 1

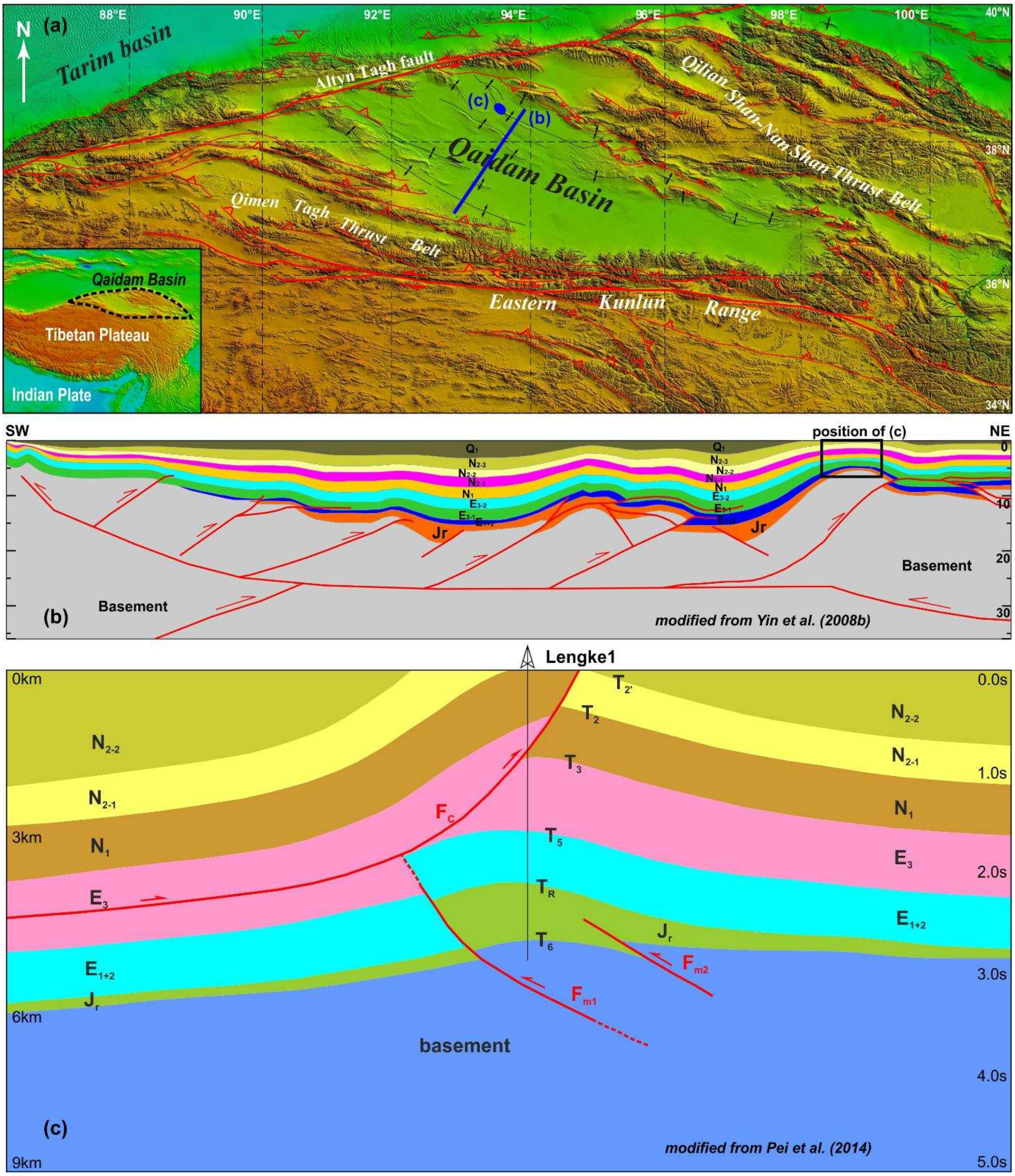

(a)
N
88°E
90°E
92°E
94°E
96°E
98°E
100°E
40°N
38°N
36°N
34°N
Tarim basin
Altyn Tagh fault
Qilian Shan-Nan Shan Thrust Belt
Qaidam Basin
(c)
(b)
Qimen Tagh Thrust Belt
Eastern Kunlun Range
Qaidam Basin
Tibetan Plateau
Indian Plate
SW
NE
position of (c)
Q1
N2-3
N2-2
N2-1
N1
E3-2
E3-1
E1+2
Jr
Basement
(b)
modified from Yin et al. (2008b)
0
10
20
30
Lengke1
0km
3km
6km
9km
0.0s
1.0s
2.0s
3.0s
4.0s
5.0s
T2'
T2
T3
T5
TR
T6
N2-2
N2-1
N1
E3
E1+2
Jr
FC
Fm1
Fm2
basement
(c)
modified from Pei et al. (2014)

4 **Figure 2**

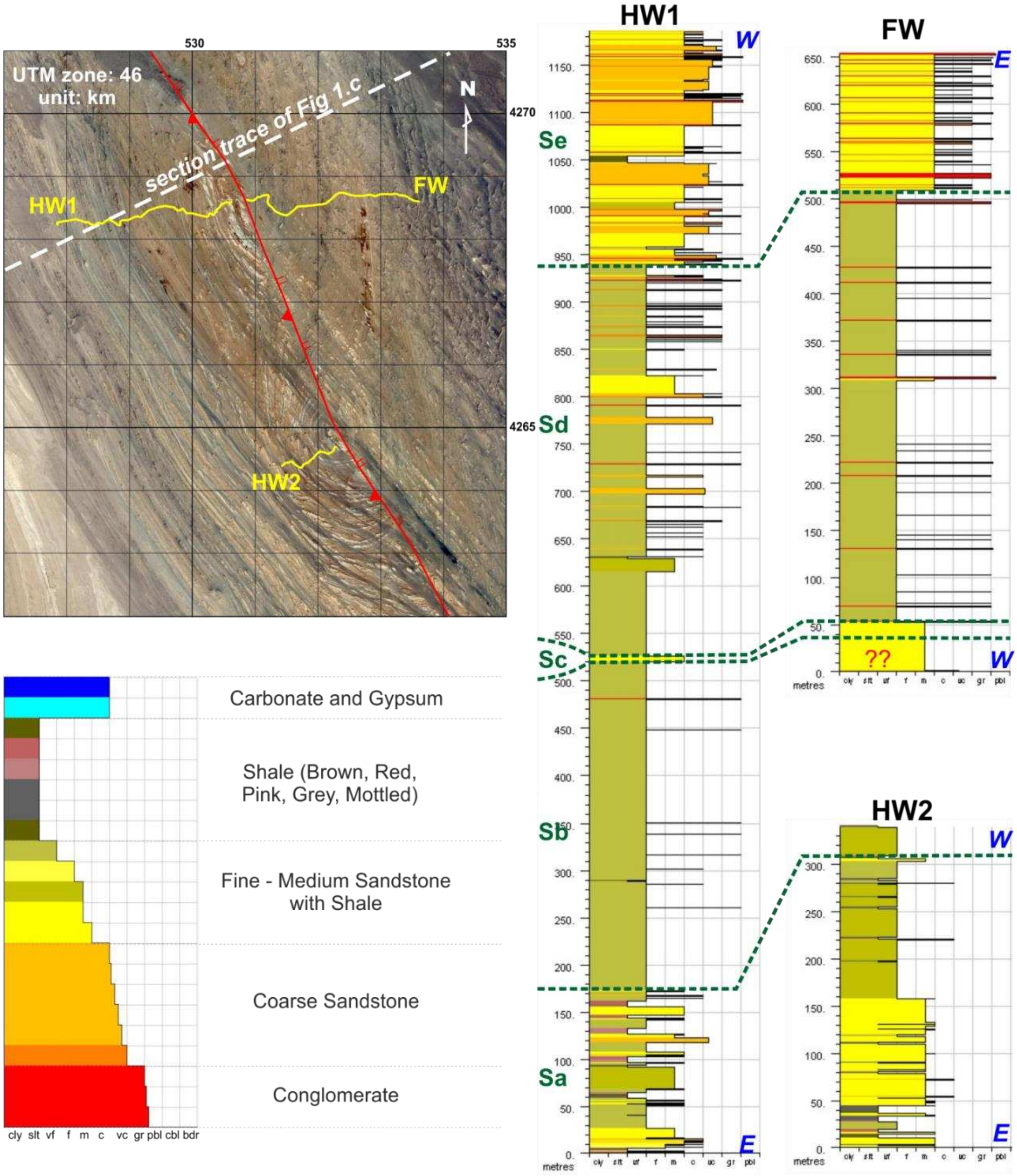

UTM zone: 46
unit: km
530
535
4270
4265
N
section trace of Fig 1.c
HW1
FW
HW2
Carbonate and Gypsum
Shale (Brown, Red, Pink, Grey, Mottled)
Fine - Medium Sandstone with Shale
Coarse Sandstone
Conglomerate
cly slt vf f m c vc gr pbl cbl bdr
HW1
W
E
Se
Sd
Sc
Sb
Sa
metres
FW
E
W
??
HW2
W
E

5

Figure 3

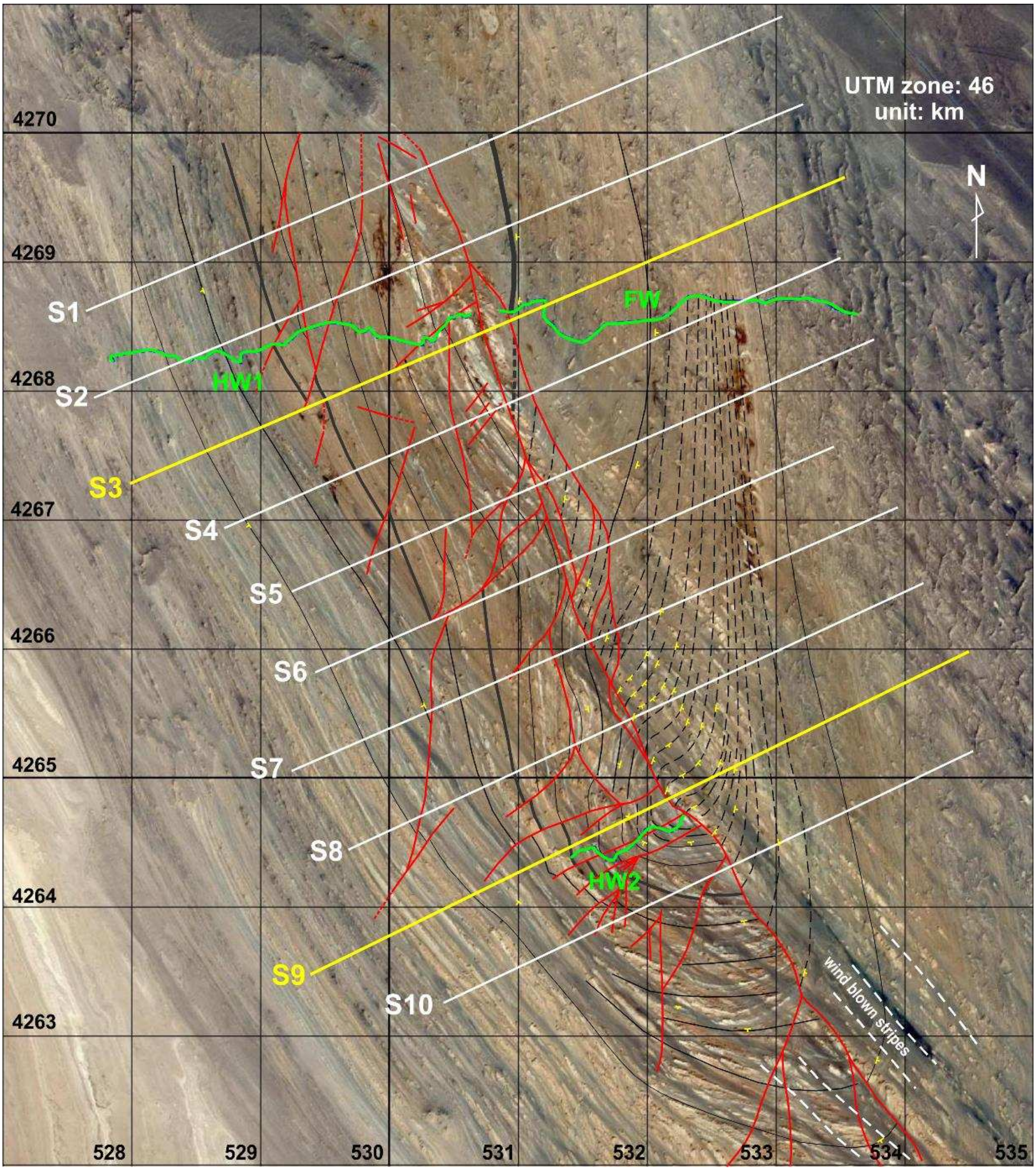
UTM zone: 46
unit: km
N
4270
4269
4268
4267
4266
4265
4264
4263
528
529
530
531
532
533
534
535
S1
S2
S3
S4
S5
S6
S7
S8
S9
S10
FW
HW1
HW2
wind blown stripes

Figure 4

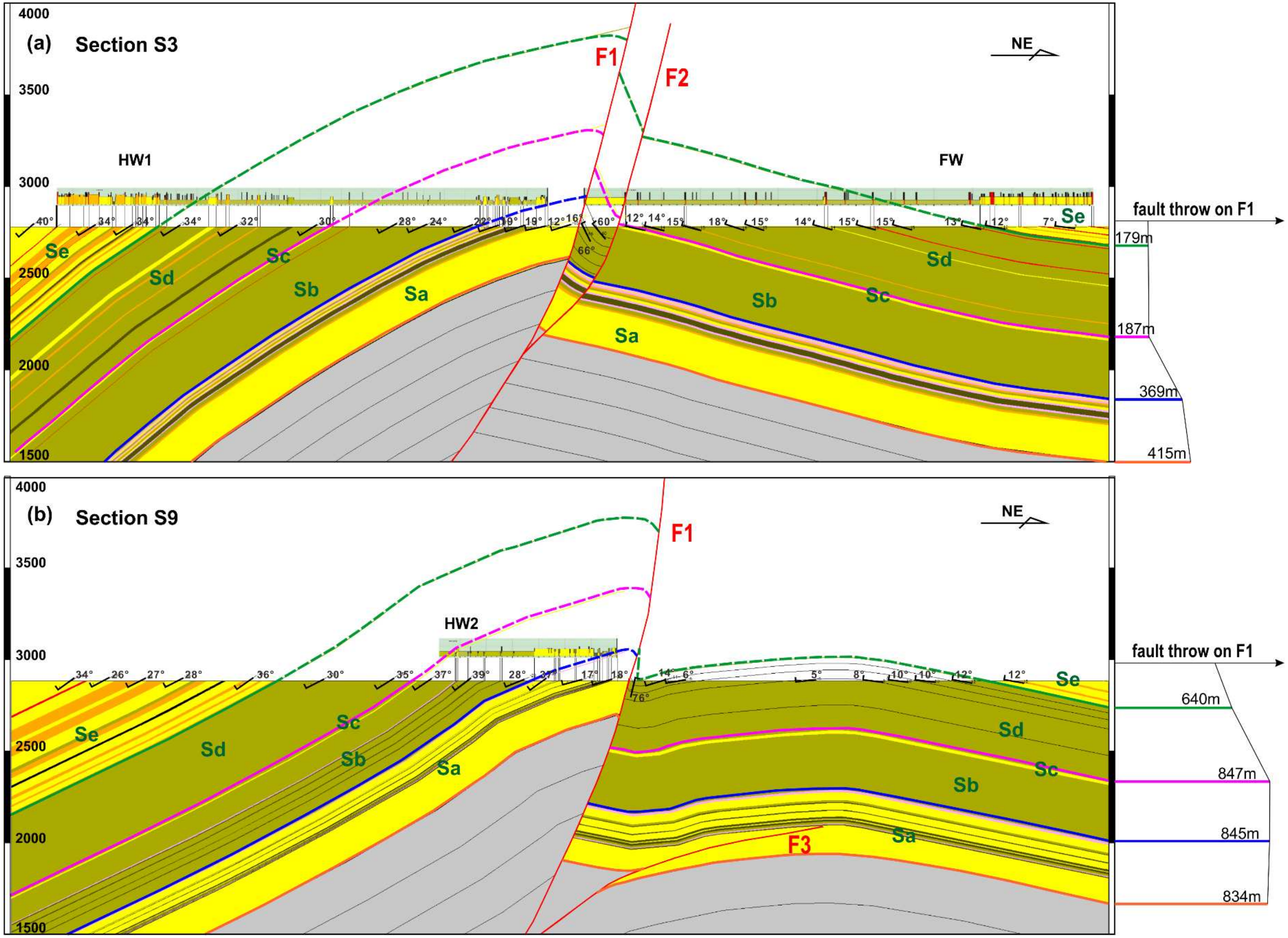
(a) Section S3
NE
F1
F2
HW1
FW
fault throw on F1
179m
187m
369m
415m
Se
Sd
Sc
Sb
Sa
4000
3500
3000
2500
2000
1500
(b) Section S9
NE
F1
F3
HW2
fault throw on F1
640m
847m
845m
834m

Figure 5

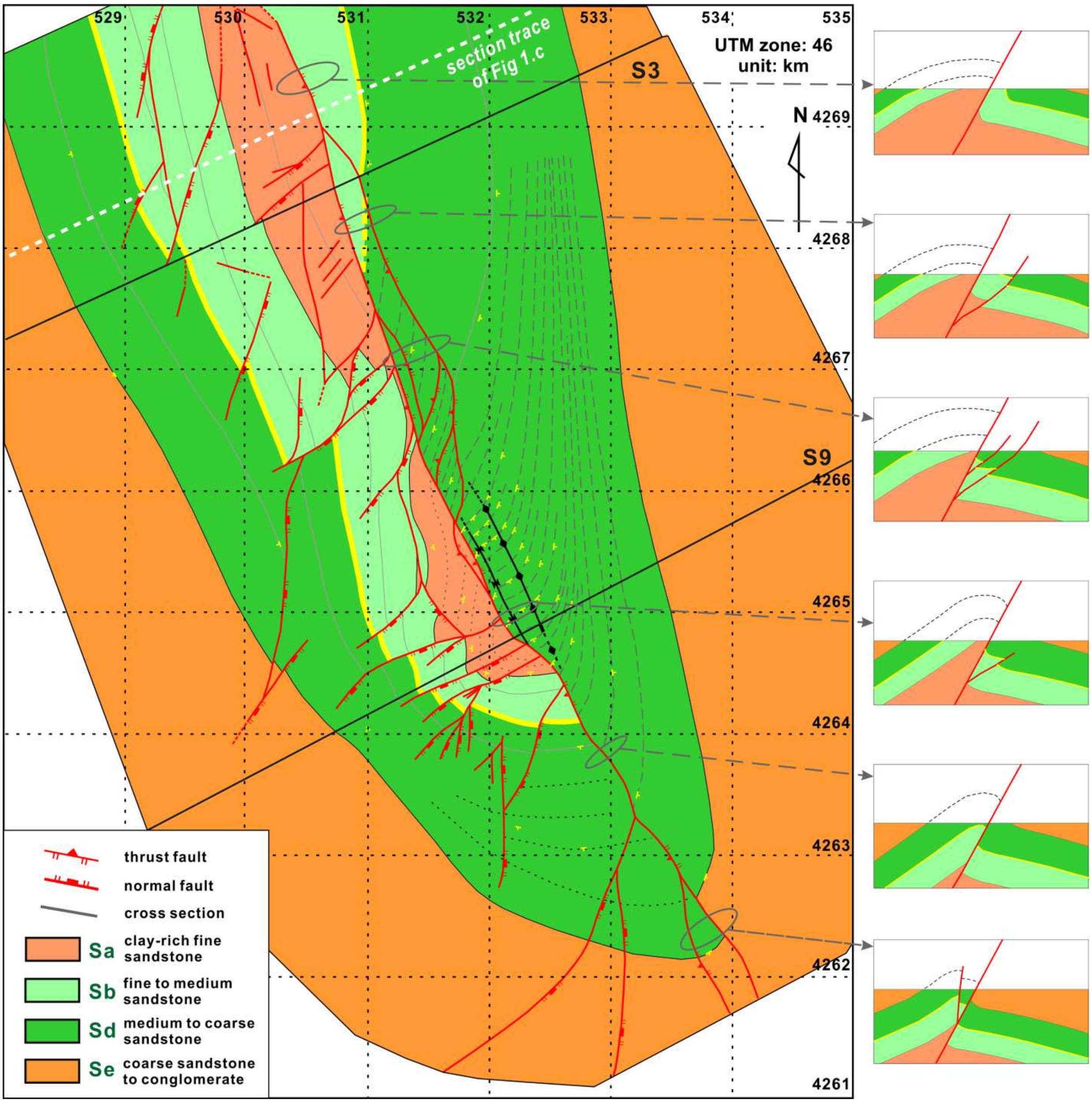

529
530
531
532
533
534
535
section trace
of Fig 1.c
S3
S9
UTM zone: 46
unit: km
N
4269
4268
4267
4266
4265
4264
4263
4262
4261
thrust fault
normal fault
cross section
Sa clay-rich fine sandstone
Sb fine to medium sandstone
Sd medium to coarse sandstone
Se coarse sandstone to conglomerate

Figure 6

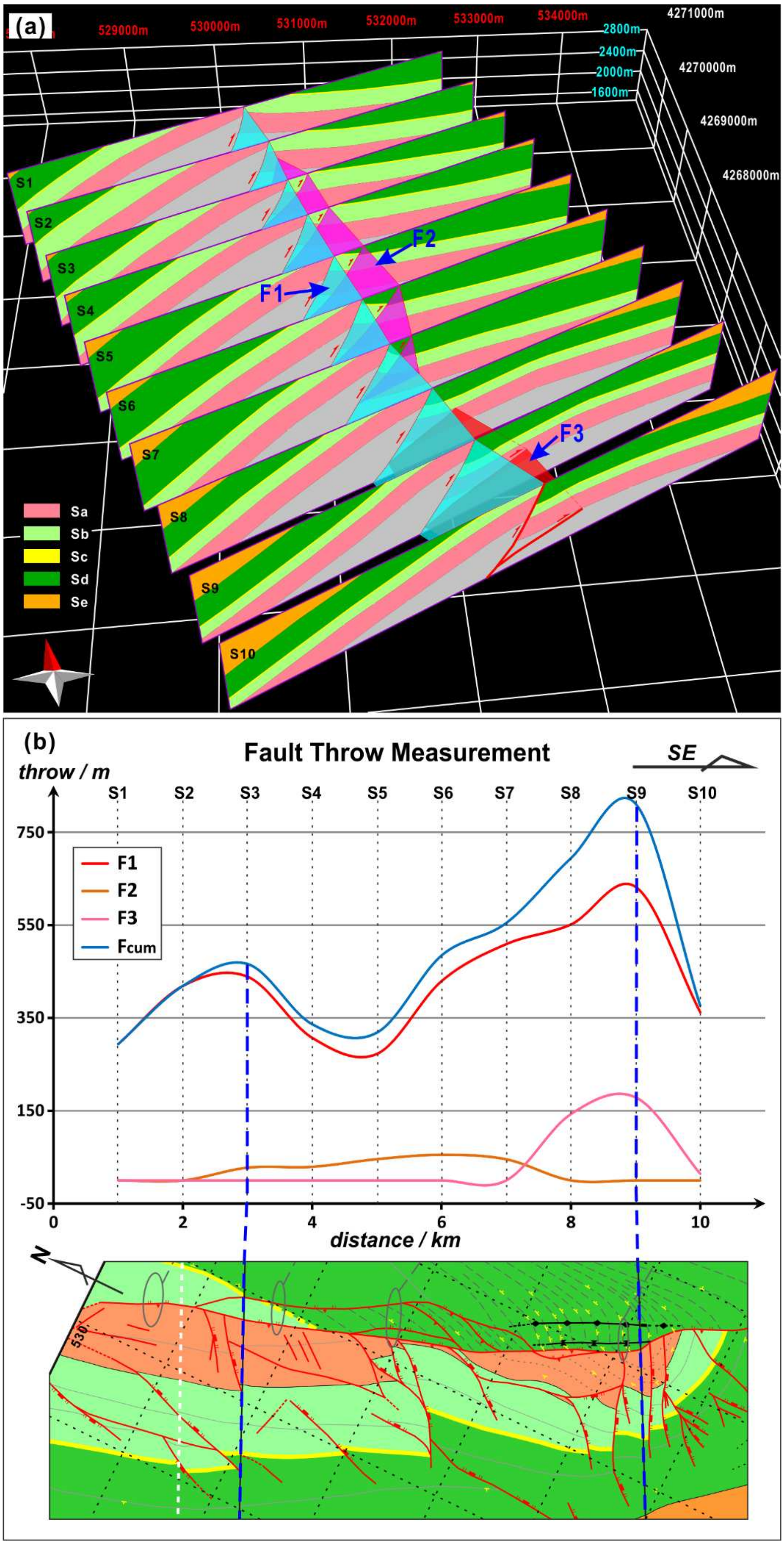
(a)
529000m
530000m
531000m
532000m
533000m
534000m
4271000m
4270000m
4269000m
4268000m
2800m
2400m
2000m
1600m
S1
S2
S3
S4
S5
S6
S7
S8
S9
S10
F1
F2
F3
Sa
Sb
Sc
Sd
Se
(b)
Fault Throw Measurement
SE
throw / m
S1
S2
S3
S4
S5
S6
S7
S8
S9
S10
750
550
350
150
-50
F1
F2
F3
Fcum
0
2
4
6
8
10
distance / km
N
530

Figure 7

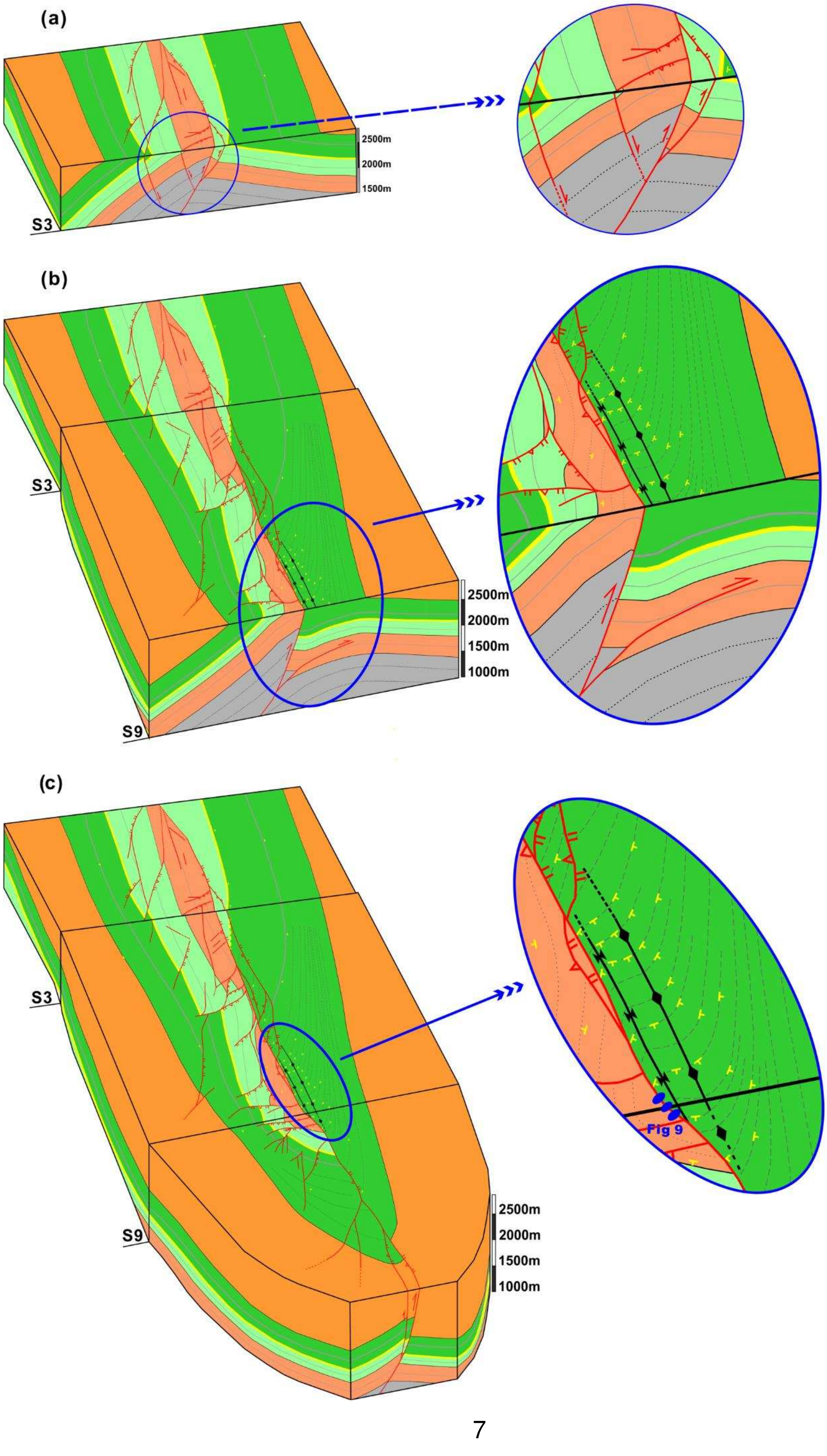
(a)
S3
2500m
2000m
1500m
(b)
S3
S9
2500m
2000m
1500m
1000m
(c)
S3
S9
2500m
2000m
1500m
1000m
Fig 9

Figure 8

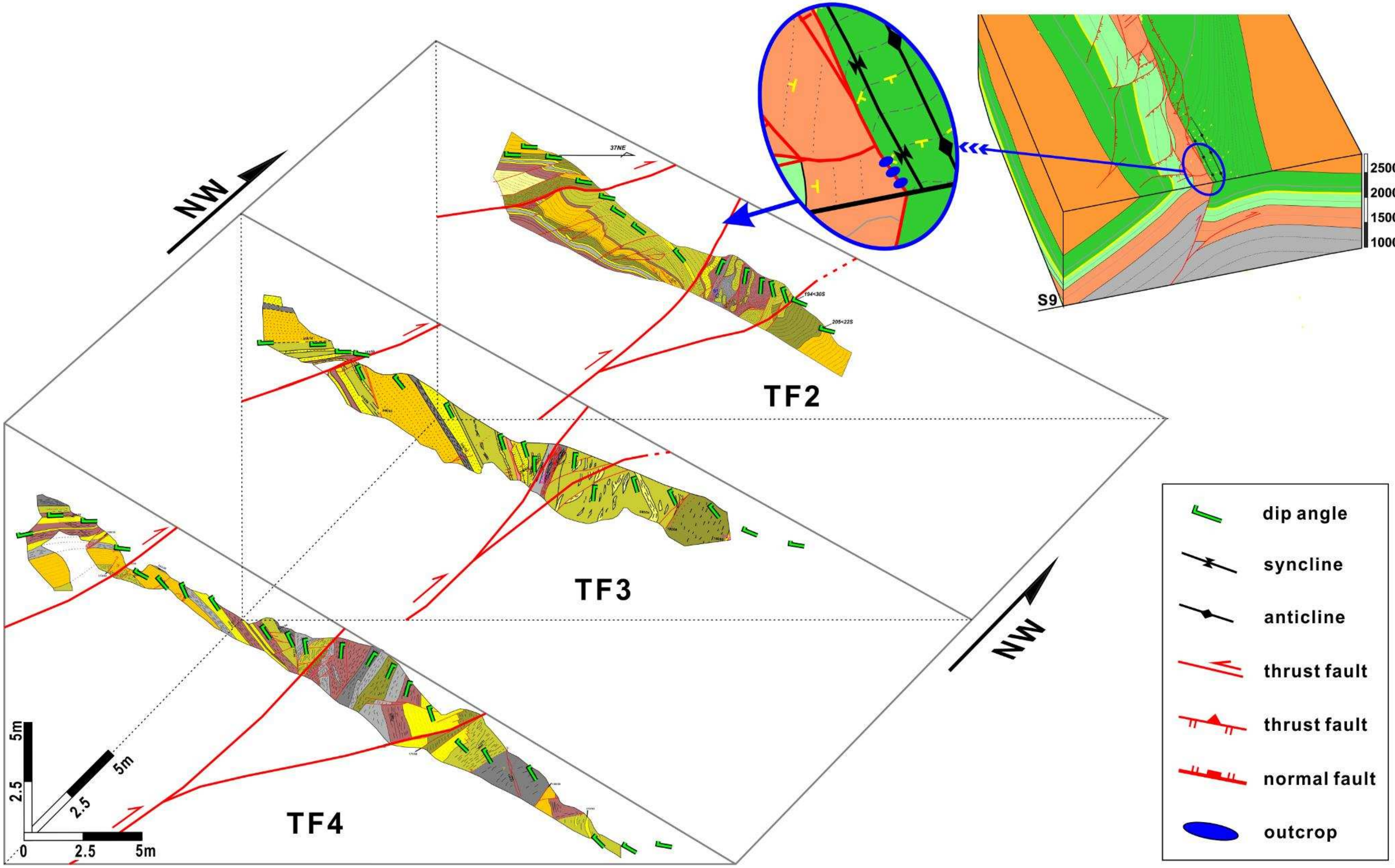
NW
NW
37NE
194<30S
205<22S
TF2
TF3
TF4
S9
2500m
2000m
1500m
1000m
5m
2.5
0
2.5
5m
5m
2.5
dip angle
syncline
anticline
thrust fault
thrust fault
normal fault
outcrop

Figure 9

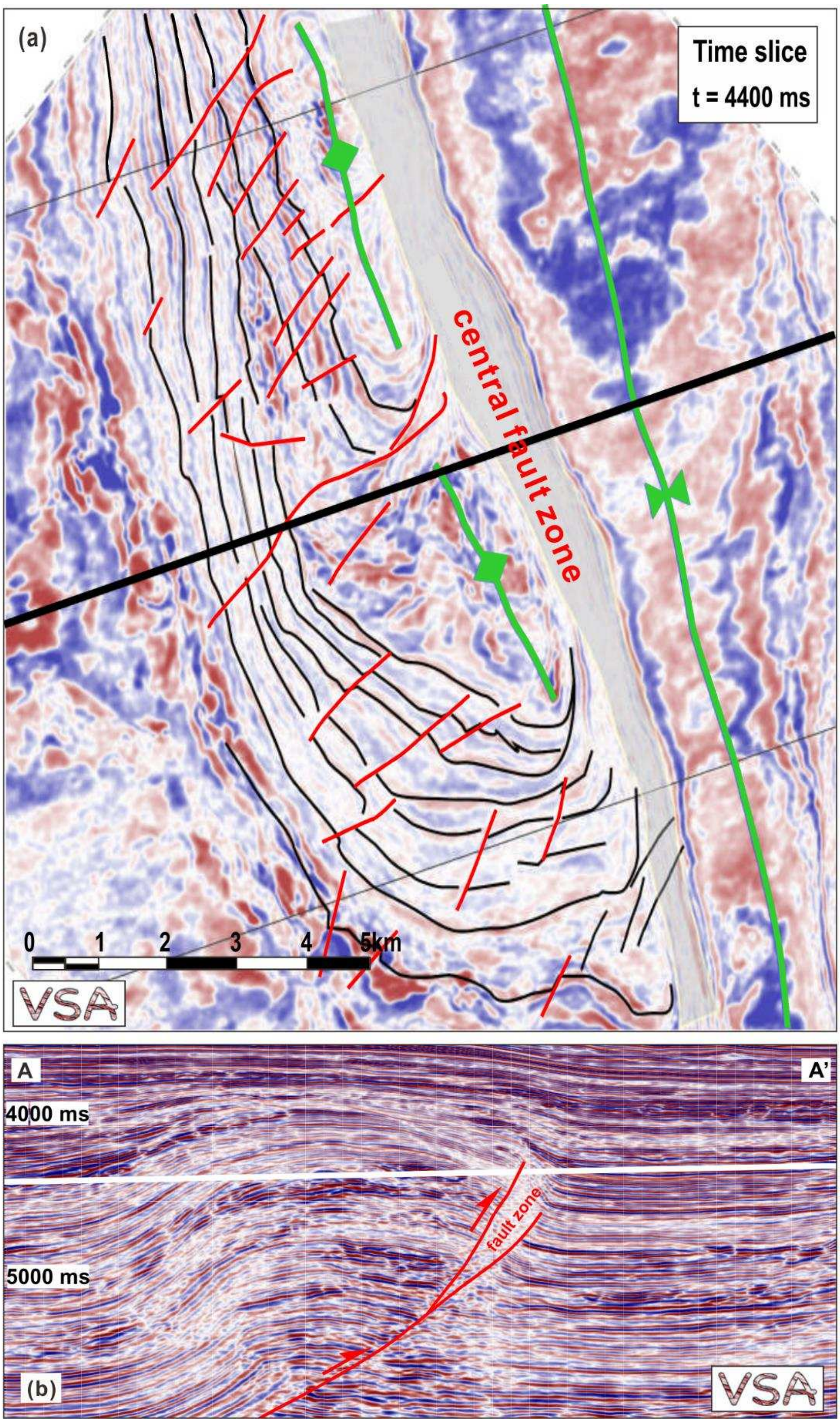

(a)
Time slice
t = 4400 ms
central fault zone
A
A'
0
1
2
3
4
5km
VSA
A
A'
4000 ms
5000 ms
fault zone
(b)
VSA

Figure 10

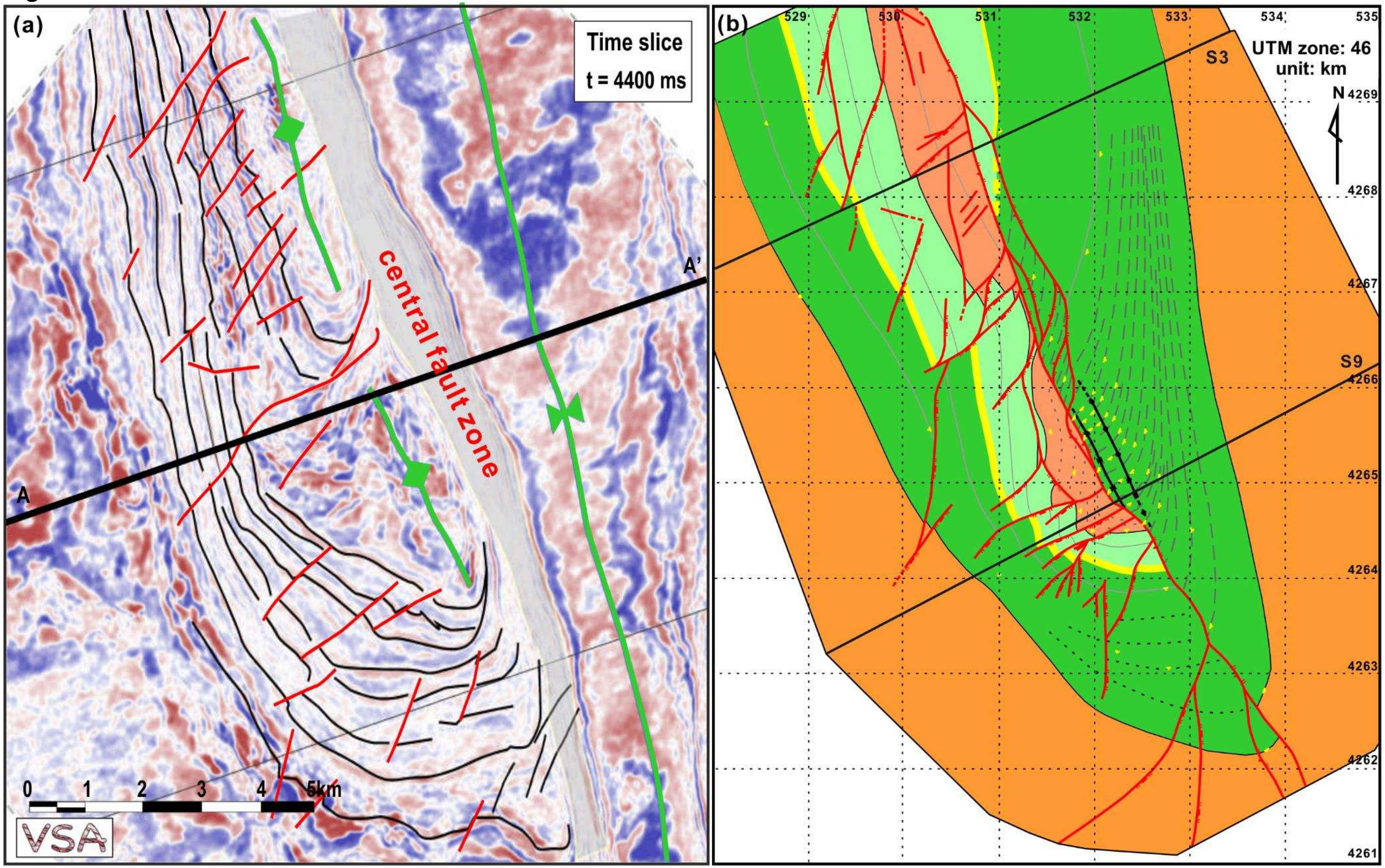
(a)
Time slice
t = 4400 ms
central fault zone
A
A'
0 1 2 3 4 5km
VSA
(b)
529 530 531 532 533 534 535
UTM zone: 46
unit: km
N
S3
S9
4269
4268
4267
4266
4265
4264
4263
4262
4261

26 **Figure 11**

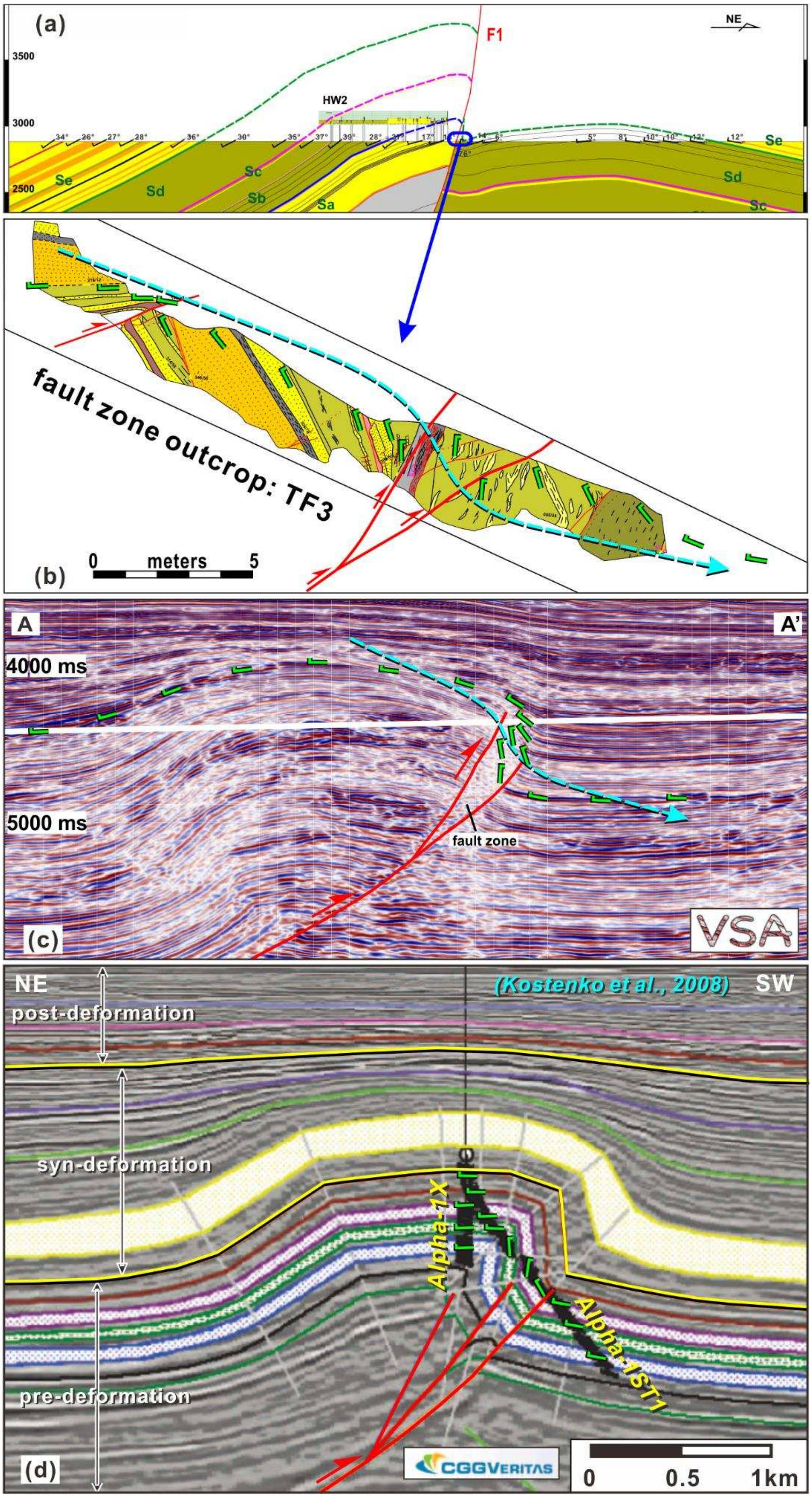

27